Aalborg Universitet

AALBORG UNIVERSITY
DENMARK

A decentralized scalable approach to voltage control of DC islanded microgrids

Tucci, Michele; Riverso, Stefano; Quintero, Juan Carlos Vasquez; Guerrero, Josep M.; Ferrari-Trecate, Giancarlo

Published in:
I E E E Transactions on Control Systems Technology

DOI (link to publication from Publisher):
10.1109/TCST.2016.2525001

Publication date:
2016

Document Version
Early version, also known as pre-print

Link to publication from Aalborg University

Citation for published version (APA):
Tucci, M., Riverso, S., Quintero, J. C. V., Guerrero, J. M., & Ferrari-Trecate, G. (2016). A decentralized scalable approach to voltage control of DC islanded microgrids. *I E E E Transactions on Control Systems Technology*, *24*(6), 1965 - 1979. https://doi.org/10.1109/TCST.2016.2525001

General rights
Copyright and moral rights for the publications made accessible in the public portal are retained by the authors and/or other copyright owners and it is a condition of accessing publications that users recognise and abide by the legal requirements associated with these rights.

- Users may download and print one copy of any publication from the public portal for the purpose of private study or research.
- You may not further distribute the material or use it for any profit-making activity or commercial gain
- You may freely distribute the URL identifying the publication in the public portal -

Take down policy
If you believe that this document breaches copyright please contact us at vbn@aub.aau.dk providing details, and we will remove access to the work immediately and investigate your claim.

Downloaded from vbn.aau.dk on: May 05, 2023

A decentralized scalable approach to voltage control of DC islanded microgrids

Michele Tucci, *Student Member, IEEE*, Stefano Riverso, *Member, IEEE*, Juan C. Vasquez, *Member, IEEE*, Josep M. Guerrero, *Fellow, IEEE*, and Giancarlo Ferrari-Trecate, *Senior Member, IEEE*

***Abstract*—We propose a new decentralized control scheme for DC Islanded microGrids (ImGs) composed by several Distributed Generation Units (DGUs) with a general interconnection topology. Each local controller regulates to a reference value the voltage of the point of common coupling of the corresponding DGU. Notably, off-line control design is conducted in a plug-and-play fashion meaning that (i) the possibility of adding/removing a DGU without spoiling stability of the overall ImG is checked through an optimization problem; (ii) when a DGU is plugged in or out at most neighboring DGUs have to update their controllers and (iii) the synthesis of a local controller uses only information on the corresponding DGU and lines connected to it. This guarantees total scalability of control synthesis as the ImG size grows or DGUs get replaced. Yet, under mild approximations of line dynamics, we formally guarantee stability of the overall closed-loop ImG. The performance of the proposed controllers is analyzed simulating different scenarios in PSCAD.**

***Index Terms*—Decentralized control, plug-and-play, DC microgrid, islanded microgrid, voltage control.**

I. Introduction

In the recent years, the increasing penetration of renewable energy sources has motivated a growing interest for microgrids, energy networks composed by the interconnection of Distributed Generation Units (DGUs) and loads [1], [2], [3]. Microgrids are self-sustained electric systems that can supply local loads even in islanded mode, i.e. disconnected from the main grid [4]. Besides their use for electrifying remote areas, islands, or large buildings, microgrids can be used for improving resilience to faults and power quality in power networks [5]. So far, research has mainly focused on AC microgrids [1], [4], [5], [6], [7]. However, technological advances in power electronics converters have considerably facilitated the operation of DC power systems. This, together with the increasing use of DC renewables (e.g. PV panels), batteries and loads (e.g. electronic appliances, LEDs and electric vehicles), has triggered a major interest in DC microgrids [8], [9], [10]. DC microgrids have also several advantages over their AC counterparts. For instance, control of reactive power or unbalanced electric signals are not an issue. On the other hand, protection of DC systems is still a challenging problem [10], [2].

For AC Islanded microGrids (ImGs) a key issue is to guarantee voltage and frequency stability by controlling inverters interfacing energy sources with lines and loads. This problem has received great attention and several decentralized control schemes have been proposed, based either on droop control [4], [11], [12], or not [13], [6], [14]. Some control design approaches are scalable, meaning that the design of a local controller for a DGU is not based on the knowledge of the whole ImG and the complexity of local control design is independent of the ImG size. In addition, the method proposed in [6], [14] allows for the seamless plugging-in, unplugging and replacement of DGUs without spoiling ImG stability. Control design procedure with these features have been termed Plug-and-Play (PnP) [15], [16], [17], [18], [19].

Voltage stability is critical also in DC microgrids as they cannot be directly coupled to an "infinite-power" source, such as the AC main grid, and therefore they always operate in islanded mode. Existing controllers for the stabilization of DC ImGs are mainly based on droop control [9], [20], [21]. Related works can be also found in the field of multi-terminal HVDC transmission systems, although for simplified converter dynamics [22] of specific network topologies [23]. So far, however, stability of the closed-loop systems has been analyzed only for specific ImGs [9], [20].

In this paper we develop a totally scalable method for the synthesis of decentralized controllers for DC ImGs. We propose a PnP design procedure where the synthesis of a local controller requires only the model of the corresponding DGU and the parameters of power lines connected to it. Importantly, no specific information about any other DGU is needed. Moreover, when a DGU is plugged in or out, only DGUs physically connected to it have to retune their local controllers. As in [6], we exploit Quasi-Stationary Line (QSL) approximations of line dynamics [24] and use separable Lyapunov functions for mapping control design into a Linear Matrix Inequality (LMI) problem. This also allows to automatically deny plugging-in/out requests if these operations spoil the stability of the ImG. Control algorithms in [6] and in the present paper share several similarities, hence showing that the combination of QSL models and separable Lyapunov functions provides a unified framework for addressing voltage stability problems both in AC and DC microgrids. This is a positive feature, given the fundamental differences in microgrid models and control aims in the AC and DC cases.

In order to validate our results, we run several simulations in PSCAD using realistic models of Buck converters and associated filters. As a first test, we consider two radially connected DGUs [25] and we show that, in spite of QSL approximations, PnP controllers lead to very good performances in terms of voltage tracking and robustness to unknown load

M. Tucci and G. Ferrari-Trecate are with Dipartimento di Ingegneria Industriale e dell'Informazione, Università degli Studi di Pavia.

S. Riverso is with United Technologies Research Center Ireland, 4th Floor, Penrose Business Center, Penrose Wharf, Cork, Ireland.

J. C. Vasquez and J. M. Guerrero are with the Institute of Energy Technology, Aalborg University, Aalborg East DK-9220, Denmark.

Corresponding author: giancarlo.ferrari@unipv.it

dynamics. We also show how to embed PnP controllers in a bumpless transfer scheme [26] so as to avoid abrupt changes of the control variables due to controller switching. Then, we consider an ImG with 5 DGUs arranged in a meshed topology including loops and discuss the real-time plugging-in and out of a DGU.

The paper is organized as follows. In Section II we present dynamical models of ImGs and the adopted line approximation. In Section III, the procedure for performing PnP operations is described. In Section IV we assess performance of PnP controllers through simulation case studies. Section V is devoted to conclusions.

II. Model of the DC Microgrid

This section discusses dynamic models of ImGs. For clarity, we start by introducing an ImG consisting of two parallel DGUs, then we generalize the model to ImGs composed of N DGUs. Consider the scheme depicted in Figure 1 comprising two DGUs denoted with i and j and connected through a DC line with an impedance specified by parameters $R_{ij} > 0$ and $L_{ij} > 0$. In each DGU, the DC voltage source represents a generic renewable resource[1] and a Buck converter is present in order to supply a local DC load connected to the Point of Common Coupling (PCC) through a series LC filter. Furthermore, we assume that loads are unknown and we treat them as current disturbances (I_L) [6], [27].

Applying Kirchoff's voltage law and Kirchoff's current law to the electrical scheme of Figure 1, leads to the following set of equations:

$$\text{DGU } i\text{:} \quad \begin{cases} \dfrac{dV_i}{dt} = \dfrac{1}{C_{ti}} I_{ti} + \dfrac{1}{C_{ti}} I_{ij} - \dfrac{1}{C_{ti}} I_{Li} & \text{(1a)} \\ \dfrac{dI_{ti}}{dt} = -\dfrac{R_{ti}}{L_{ti}} I_{ti} - \dfrac{1}{L_{ti}} V_i + \dfrac{1}{L_{ti}} V_{ti} & \text{(1b)} \end{cases}$$

$$\text{Line } ij\text{:} \quad \left\{ L_{ij} \frac{dI_{ij}}{dt} = V_j - R_{ij} I_{ij} - V_i \right. \qquad \text{(1c)}$$

$$\text{Line } ji\text{:} \quad \left\{ L_{ji} \frac{dI_{ji}}{dt} = V_i - R_{ji} I_{ji} - V_j \right. \qquad \text{(1d)}$$

$$\text{DGU } j\text{:} \quad \begin{cases} \dfrac{dV_j}{dt} = \dfrac{1}{C_{tj}} I_{tj} + \dfrac{1}{C_{tj}} I_{ji} - \dfrac{1}{C_{tj}} I_{Lj} & \text{(1e)} \\ \dfrac{dI_{tj}}{dt} = -\dfrac{R_{tj}}{L_{tj}} I_{tj} - \dfrac{1}{L_{tj}} V_j + \dfrac{1}{L_{tj}} V_{tj} & \text{(1f)} \end{cases}$$

As in [6], we notice that from (1c) and (1d) one gets two opposite line currents I_{ij} and I_{ji}. This is equivalent to have a reference current entering in each DGU. We exploit the following assumption to ensure that $I_{ij}(t) = -I_{ji}(t)$, $\forall t \geq 0$.

Assumption 1. *Initial states for the line currents fulfill* $I_{ij}(0) = -I_{ji}(0)$. *Furthermore, we set* $L_{ij} = L_{ji}$ *and* $R_{ij} = R_{ji}$.

Remark 1. *According to the terminology in Section 3.4 of [28], the system in* (1c), (1d) *represents an expansion of the line model one obtains introducing only a single state variable. System* (1) *can also be viewed as a system of differential-algebraic equations, given by (1a)-(1c), (1e), (1f) and* $I_{ij}(t) = -I_{ji}(t)$.

At this point, we notice that adopting the above notation for the lines, both DGU models have the same structure. In particular, by recalling that the load current I_{L*}, $* \in \{i, j\}$ is treated as a disturbance, from (1) we obtain the following linear system

$$\begin{aligned} \dot{x}(t) &= Ax(t) + Bu(t) + Md(t) \\ y(t) &= Cx(t) \end{aligned} \qquad (2)$$

where $x = [V_i, I_{ti}, I_{ij}, I_{ji}, V_{j,}, I_{tj}]^T$ is the state, $u = [V_{ti}, V_{tj}]^T$ the input, $d = [I_{Li}, I_{Lj}]^T$ the disturbance and $y = [V_i, V_j]^T$ the output of the system. All matrices in (2), which are obtained from (1), are given in Appendix A.1 of [29].

Next, we show how to describe each DGU as a dynamical system affected directly by state of the other DGU connected to it. An approximate model will be proposed so that there will be no need of using the line current in the DGU state equations.

A. QSL model

As in [24] and [30], we assume L_{ij} and L_{ji} are small enough so as to replace the left-hand side of (1c) and (1d) with zero. Consequently, from (1c) and (1d), one gets the QSL model

$$\bar{I}_{ij} = \frac{V_j}{R_{ij}} - \frac{V_i}{R_{ij}} \qquad \text{(3a)}$$

$$\bar{I}_{ji} = \frac{V_i}{R_{ji}} - \frac{V_j}{R_{ji}} \qquad \text{(3b)}$$

By replacing variable I_{ij} in (1a) with the right-hand side of (3a), we obtain the following model of DGU i

$$\text{DGU } i: \quad \begin{cases} \dfrac{dV_i}{dt} = \dfrac{1}{C_{ti}} I_{ti} + \dfrac{V_j}{C_{ti} R_{ij}} - \dfrac{V_i}{C_{ti} R_{ij}} - \dfrac{1}{C_{ti}} I_{Li} \\ \dfrac{dI_{ti}}{dt} = -\dfrac{1}{L_{ti}} V_i - \dfrac{R_{ti}}{L_{ti}} I_{ti} + \dfrac{1}{L_{ti}} V_{ti} \end{cases} \qquad (4)$$

Switching indexes i and j in (4) gives the model of DGU j. It can be equivalently derived by substituting I_{ji} in (1e) with the right-hand side of (3b). In a more compact form, the dynamics of DGU i is

$$\Sigma_{[i]}^{DGU}: \begin{cases} \dot{x}_{[i]}(t) = A_{ii} x_{[i]}(t) + B_i u_{[i]}(t) + M_i d_{[i]}(t) + \xi_{[i]}(t) \\ y_{[i]}(t) = C_i x_{[i]}(t) \\ z_{[i]}(t) = H_i y_{[i]}(t) \end{cases} \qquad (5)$$

where $x_{[i]} = [V_i, I_{ti}]^T$ is the state, $u_{[i]} = V_{ti}$ the control input, $d_{[i]} = I_{Li}$ the exogenous input and $z_{[i]} = V_i$ the controlled variable of the system. Moreover, $y_{[i]}(t)$ is the measurable output and we assume $y_{[i]} = x_{[i]}$, while $\xi_{[i]}(t) = A_{ij} x_{[j]}$ represents the coupling with DGU j.

The matrices of $\Sigma_{[i]}^{DGU}$ are obtained from (4) and they are here provided:

[1]This approximation is justified by the observation that changes in the power supplied by renewables take place at a timescale which is slower than the one we are interested in for stability analysis. Moreover, renewables are usually equipped with storage units damping stochastic fluctuations.

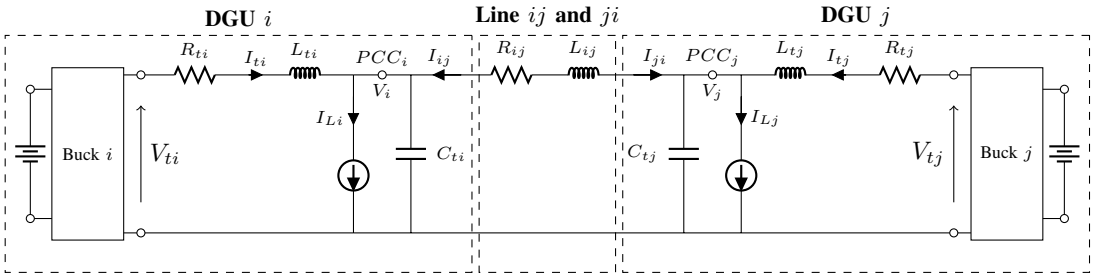

Fig. 1: Electrical scheme of a DC ImG composed of two radially connected DGUs with unmodeled loads.

$$A_{ii} = \begin{bmatrix} -\frac{1}{R_{ij}C_{ti}} & \frac{1}{C_{ti}} \\ -\frac{1}{L_{ti}} & -\frac{R_{ti}}{L_{ti}} \end{bmatrix} \quad A_{ij} = \begin{bmatrix} \frac{1}{R_{ij}C_{ti}} & 0 \\ 0 & 0 \end{bmatrix}$$

$$B_i = \begin{bmatrix} 0 \\ \frac{1}{L_{ti}} \end{bmatrix} \quad M_i = \begin{bmatrix} -\frac{1}{C_{ti}} \\ 0 \end{bmatrix} \quad C_i = \begin{bmatrix} 1 & 0 \\ 0 & 1 \end{bmatrix} \quad H_i = \begin{bmatrix} 1 & 0 \end{bmatrix}.$$

We have now all the ingredients to write the QSL model of the overall microgrid depicted in Figure 1. In particular, from (5), we get

$$\begin{aligned} \begin{bmatrix} \dot{x}_{[i]} \\ \dot{x}_{[j]} \end{bmatrix} &= A \begin{bmatrix} x_{[i]} \\ x_{[j]} \end{bmatrix} + \begin{bmatrix} B_i & 0 \\ 0 & B_j \end{bmatrix} \begin{bmatrix} u_{[i]} \\ u_{[j]} \end{bmatrix} + \begin{bmatrix} M_i & 0 \\ 0 & M_j \end{bmatrix} \begin{bmatrix} d_{[i]} \\ d_{[j]} \end{bmatrix} \\ \begin{bmatrix} y_{[i]} \\ y_{[j]} \end{bmatrix} &= \begin{bmatrix} C_i & 0 \\ 0 & C_j \end{bmatrix} \begin{bmatrix} x_{[i]} \\ x_{[j]} \end{bmatrix} \\ \begin{bmatrix} z_{[i]} \\ z_{[j]} \end{bmatrix} &= \begin{bmatrix} H_i & 0 \\ 0 & H_j \end{bmatrix} \begin{bmatrix} y_{[i]} \\ y_{[j]} \end{bmatrix} \end{aligned} \tag{6}$$

where

$$A = \begin{bmatrix} A_{ii} & A_{ij} \\ A_{ji} & A_{jj} \end{bmatrix}.$$

Remark 2. *We will show in Section III-C that QSL approximation can be justified in terms of singular perturbation theory [31], [32], [33], [34]. In other words, stabilization of* (6) *will imply stabilization of* (1)*, for sufficiently small line inductances.*

We notice that A is block-triangular. Moreover, by construction, $A_{ll,ij} = A_{ll,ji} < 0$. Then, for stability analysis, line dynamics can be neglected and just the system composed by $\Sigma_{[i]}^{DGU}$ and $\Sigma_{[j]}^{DGU}$ (giving rise to the upper-left block of matrix A) matters. We will refer to it as QSL-ImG model.

B. QSL model of a microgrid composed of N DGUs

In this section, a generalization of model (5) to ImGs composed of N DGUs is presented. Let $\mathcal{D} = \{1, \dots, N\}$. First, we call two DGUs neighbors if there is a power line connecting them. Then, we denote with $\mathcal{N}_i \subset \mathcal{D}$ the subset of neighbors of DGU i. We highlight that the neighboring relation is symmetric, consequently $j \in \mathcal{N}_i$ implies $i \in \mathcal{N}_j$. Furthermore, let $\mathcal{E} = \{(i,j) : i \in \mathcal{D},\ j \in \mathcal{N}_i\}$ collect pairs of indices associated to lines[2]. In this setting, the whole ImG model is obtained

- modeling each DGU i, $i \in \mathcal{D}$, as in (1a)-(1b) after replacing I_{ij} with $\sum_{j \in \mathcal{N}_i} I_{ij}$;
- modeling each line $(i,j) \in \mathcal{E}$ as in (1c).

However, if QSL approximations of all lines $(i,j) \in \mathcal{E}$ are used, the ImG is described only by subsystems (5) with $\xi_{[i]} = \sum_{j \in \mathcal{N}_i} A_{ij} x_{[j]}(t)$. All matrices appearing in (5) do not change, with the exception of A_{ii} that becomes

$$A_{ii} = \begin{bmatrix} \sum_{j \in \mathcal{N}_i} -\frac{1}{R_{ij}C_{ti}} & \frac{1}{C_{ti}} \\ -\frac{1}{L_{ti}} & -\frac{R_{ti}}{L_{ti}} \end{bmatrix}. \tag{7}$$

The overall QSL-ImG model can be written as follows

$$\dot{\mathbf{x}}(t) = \mathbf{A}\mathbf{x}(t) + \mathbf{B}\mathbf{u}(t) + \mathbf{M}\mathbf{d}(t) \tag{8}$$

$$\begin{aligned} \mathbf{y}(t) &= \mathbf{C}\mathbf{x}(t) \\ \mathbf{z}(t) &= \mathbf{H}\mathbf{y}(t) \end{aligned} \tag{9}$$

where $\mathbf{x} = (x_{[1]}, \dots, x_{[N]}) \in \mathbb{R}^{2N}$, $\mathbf{u} = (u_{[1]}, \dots, u_{[N]}) \in \mathbb{R}^N$, $\mathbf{d} = (d_{[1]}, \dots, d_{[N]}) \in \mathbb{R}^N$, $\mathbf{y} = (y_{[1]}, \dots, y_{[N]}) \in \mathbb{R}^{2N}$, $\mathbf{z} = (z_{[1]}, \dots, z_{[N]}) \in \mathbb{R}^N$. Matrices $\mathbf{A}$, $\mathbf{B}$, $\mathbf{M}$, $\mathbf{C}$ and $\mathbf{H}$ are reported in Appendix A.2 and A.3 of [29].

Comments in Remark 2 apply also here: in Section III-C, we will show that the QSL-ImG model can be justified treating inductances L_{ij}, $(i,j) \in \mathcal{E}$, as perturbation parameters and resorting to singular perturbation theory.

III. Plug-and-Play decentralized voltage control

A. Decentralized control scheme with integrators

Let $\mathbf{z_{ref}}(t)$ denote the constant desired reference trajectory for the output $\mathbf{z}(t)$. In order to track asymptotically $\mathbf{z_{ref}}(t)$ when $\mathbf{d}(t)$ is constant, we consider the augmented ImG model with integrators [35]. A necessary condition for having that the steady-state error $\mathbf{e}(t) = \mathbf{z_{ref}}(t) - \mathbf{z}(t)$ tends to zero as $t \to \infty$, is that, for arbitrary constant signals $\mathbf{d}(t) = \bar{\mathbf{d}}$ and $\mathbf{z_{ref}}(t) = \bar{\mathbf{z}}_{\mathbf{ref}}$, there are equilibrium states and inputs $\bar{\mathbf{x}}$ and $\bar{\mathbf{u}}$ verifying

$$\begin{aligned} \mathbf{0} &= \mathbf{A}\bar{\mathbf{x}} + \mathbf{B}\bar{\mathbf{u}} + \mathbf{M}\bar{\mathbf{d}} \\ \bar{\mathbf{z}}_{\mathbf{ref}} &= \mathbf{H}\mathbf{C}\bar{\mathbf{x}} \end{aligned} \tag{10}$$

$$\Gamma \begin{bmatrix} \bar{\mathbf{x}} \\ \bar{\mathbf{u}} \end{bmatrix} = \begin{bmatrix} \mathbf{0} & -\mathbf{M} \\ \mathbf{I} & \mathbf{0} \end{bmatrix} \begin{bmatrix} \bar{\mathbf{z}}_{\mathbf{ref}} \\ \bar{\mathbf{d}} \end{bmatrix}, \quad \Gamma = \begin{bmatrix} \mathbf{A} & \mathbf{B} \\ \mathbf{HC} & \mathbf{0} \end{bmatrix} \in \mathbb{R}^{3N \times 3N} \tag{11}$$

[2]Note that we consider (i,j) an ordered pair and therefore, from the symmetry of the neighboring relation, if $(i,j) \in \mathcal{E}$ then also $(j,i) \in \mathcal{E}$.

Proposition 1. *Given* $\bar{\mathbf{z}}_{\mathbf{ref}}$ *and* $\bar{\mathbf{d}}$*, vectors* $\bar{\mathbf{x}}$ *and* $\bar{\mathbf{u}}$ *satisfying* (11) *always exist.*

Proof. From [35], we know that there exist $\bar{\mathbf{x}}, \bar{\mathbf{u}}$ verifying (11) if and only if the following two conditions are fulfilled:

(i) The number of controlled variables is not greater than the number of control inputs.
(ii) The system under control has no invariant zeros (i.e. $\text{rank}(\Gamma) = 3N$).

Condition (i) is fulfilled since from (5) one has that $u_{[i]}$ and $z_{[i]}$ have the same size, $\forall i \in \mathcal{D}$. In order to prove Condition (ii), we exploit the definition of matrices $\mathbf{A}$, $\mathbf{B}$, $\mathbf{C}$ and $\mathbf{H}$ and the fact that electrical parameters are positive. □

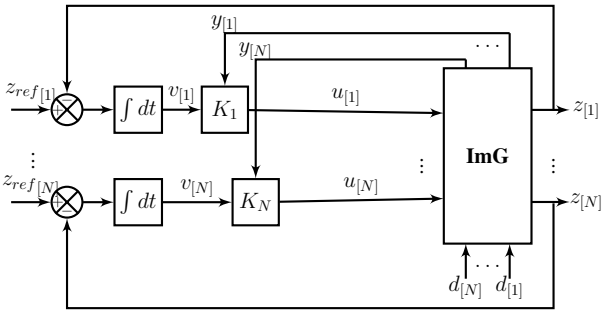

Fig. 2: Control scheme with integrators for the overall augmented model.

The dynamics of the integrators is (see Figure 2)

$$\begin{aligned} \dot{v}_i(t) = e_{[i]}(t) &= z_{ref_{[i]}}(t) - z_{[i]}(t) \\ &= z_{ref_{[i]}}(t) - H_i C_i x_{[i]}(t), \end{aligned} \tag{12}$$

and hence, the DGU model augmented with integrators is

$$\hat{\Sigma}^{DGU}_{[i]} : \begin{cases} \dot{\hat{x}}_{[i]}(t) = \hat{A}_{ii}\hat{x}_{[i]}(t) + \hat{B}_i u_{[i]}(t) + \hat{M}_i \hat{d}_{[i]}(t) + \hat{\xi}_{[i]}(t) \\ \hat{y}_{[i]}(t) = \hat{C}_i \hat{x}_{[i]}(t) \\ z_{[i]}(t) = \hat{H}_i \hat{y}_{[i]}(t) \end{cases} \tag{13}$$

where $\hat{x}_{[i]} = [x^T{}_{[i]}, v_{i,}]^T \in \mathbb{R}^3$ is the state, $\hat{y}_{[i]} = \hat{x}_{[i]} \in \mathbb{R}^3$ is the measurable output, $\hat{d}_{[i]} = [d_{[i]}, z_{ref\,[i]}]^T \in \mathbb{R}^2$ collects the exogenous signals (both current of the load and reference signals) and $\hat{\xi}_{[i]}(t) = \sum_{j \in \mathcal{N}_i} \hat{A}_{ij}\hat{x}_{[j]}(t)$. Matrices in (13) are defined as follows

$$\begin{aligned} &\hat{A}_{ii} = \begin{bmatrix} A_{ii} & 0 \\ -H_i C_i & 0 \end{bmatrix} \hat{A}_{ij} = \begin{bmatrix} A_{ij} & 0 \\ 0 & 0 \end{bmatrix} \hat{B}_i = \begin{bmatrix} B_i \\ 0 \end{bmatrix} \hat{C}_i = \begin{bmatrix} C_i & 0 \\ 0 & I \end{bmatrix} \\ &\hat{M}_i = \begin{bmatrix} M_i & 0 \\ 0 & 1 \end{bmatrix} \qquad \hat{H}_i = \begin{bmatrix} H_i & 0 \end{bmatrix}. \end{aligned} \tag{14}$$

Through the following Proposition we make sure that the pair $(\hat{A}_{ii}, \hat{B}_i)$ is controllable, thus system (13) can be stabilized.

Proposition 2. *The pair* $(\hat{A}_{ii}, \hat{B}_i)$ *is controllable.*

Proof. Using the definition of controllability matrix, we get

$$\begin{aligned} \hat{M}_i^C &= \begin{bmatrix} \hat{B}_i & \hat{A}_{ii}\hat{B}_i & \hat{A}_{ii}^2\hat{B}_i \end{bmatrix} \\ &= \underbrace{\begin{bmatrix} A_{ii} & B_i \\ -H_i C_i & 0 \end{bmatrix}}_{\hat{M}^C_{i,1}} \underbrace{\begin{bmatrix} 0 & B_i & A_{ii}B_i & A_{ii}^2 B_i \\ I & 0 & 0 & 0 \end{bmatrix}}_{\hat{M}^C_{i,2}}. \end{aligned} \tag{15}$$

Matrices $\hat{M}^C_{i,1}$ and $\hat{M}^C_{i,2}$ have always full rank, since all electrical parameters are positive, hence $\text{rank}(\hat{M}_i^C) = 3$. Therefore the pair $(\hat{A}_{ii}, \hat{B}_i)$ is controllable. □

The overall augmented system is obtained from (13) as

$$\begin{cases} \dot{\hat{\mathbf{x}}}(t) = \hat{\mathbf{A}}\hat{\mathbf{x}}(t) + \hat{\mathbf{B}}\mathbf{u}(t) + \hat{\mathbf{M}}\hat{\mathbf{d}}(t) \\ \hat{\mathbf{y}}(t) = \hat{\mathbf{C}}\hat{\mathbf{x}}(t) \\ \mathbf{z}(t) = \hat{\mathbf{H}}\hat{\mathbf{y}}(t) \end{cases} \tag{16}$$

where $\hat{\mathbf{x}}$, $\hat{\mathbf{y}}$ and $\hat{\mathbf{d}}$ collect variables $\hat{x}_{[i]}$, $\hat{y}_{[i]}$ and $\hat{d}_{[i]}$ respectively, and matrices $\hat{\mathbf{A}}, \hat{\mathbf{B}}, \hat{\mathbf{C}}, \hat{\mathbf{M}}$ and $\hat{\mathbf{H}}$ are obtained from systems (13).

B. Decentralized PnP control

This section presents the adopted control approach that allows us to design local controllers while guaranteeing asymptotic stability for the augmented system (16). Local controllers are synthesized in a decentralized fashion permitting PnP operations. Let us equip each DGU $\hat{\Sigma}^{DGU}_{[i]}$ with the following state-feedback controller

$$\mathcal{C}_{[i]} : \qquad u_{[i]}(t) = K_i \hat{y}_{[i]}(t) = K_i \hat{x}_{[i]}(t) \tag{17}$$

where $K_i \in \mathbb{R}^{1\times 3}$ and controllers $\mathcal{C}_{[i]}$, $i \in \mathcal{D}$ are decentralized since the computation of $u_{[i]}(t)$ requires the state of $\hat{\Sigma}^{DGU}_{[i]}$ only. Let nominal subsystems be given by $\hat{\Sigma}^{DGU}_{[i]}$ without coupling terms $\hat{\xi}_{[i]}(t)$. We aim to design local controllers $\mathcal{C}_{[i]}$ such that the nominal closed-loop subsystem

$$\begin{cases} \dot{\hat{x}}_{[i]}(t) = (\hat{A}_{ii} + \hat{B}_i K_i)\hat{x}_{[i]}(t) + \hat{M}_i \hat{d}_{[i]}(t) \\ \hat{y}_{[i]}(t) = \hat{C}_i \hat{x}_{[i]}(t) \\ z_{[i]}(t) = \hat{H}_i \hat{y}_{[i]}(t) \end{cases} \tag{18}$$

is asymptotically stable. From Lyapunov theory, we know that if there exists a symmetric matrix $P_i \in \mathbb{R}^{3\times 3}, P_i > 0$ such that

$$(\hat{A}_{ii} + \hat{B}_i K_i)^T P_i + P_i(\hat{A}_{ii} + \hat{B}_i K_i) < 0, \tag{19}$$

then the nominal closed-loop subsystem equipped with controller $\mathcal{C}_{[i]}$ is asymptotically stable. Similarly, consider the following closed-loop QSL-ImG model obtained from (16) and (17)

$$\begin{cases} \dot{\hat{\mathbf{x}}}(t) = (\hat{\mathbf{A}} + \hat{\mathbf{B}}\mathbf{K})\hat{\mathbf{x}}(t) + \hat{\mathbf{M}}\hat{\mathbf{d}}(t) \\ \hat{\mathbf{y}}(t) = \hat{\mathbf{C}}\hat{\mathbf{x}}(t) \\ \mathbf{z}(t) = \hat{\mathbf{H}}\hat{\mathbf{y}}(t) \end{cases} \tag{20}$$

where $\hat{\mathbf{A}}$, $\hat{\mathbf{B}}$ and $\mathbf{K}$ collect matrices $\hat{A}_{ij}$, $\hat{B}_i$ and K_i, for all $i,\ j \in \mathcal{D}$. Then, (20) is asymptotically stable if matrix $\mathbf{P} = \text{diag}(P_1, \ldots, P_N)$ satisfies

$$(\hat{\mathbf{A}} + \hat{\mathbf{B}}\mathbf{K})^T \mathbf{P} + \mathbf{P}(\hat{\mathbf{A}} + \hat{\mathbf{B}}\mathbf{K}) < 0 \tag{21}$$

We want to emphasize that, in general, (19) does not imply (21). Indeed, decentralized design of local controllers can fail to guarantee voltage stability of the whole ImG, if coupling among DGUs is neglected. In order to derive conditions such that (19) guarantees (21), we first define $\hat{\mathbf{A}}_{\mathbf{D}} = \text{diag}(\hat{A}_{ii}, \ldots, \hat{A}_{NN})$ and $\hat{\mathbf{A}}_{\mathbf{C}} = \hat{\mathbf{A}} - \hat{\mathbf{A}}_{\mathbf{D}}$. Then, we

exploit the following assumptions to ensure asymptotic stability of the closed-loop QSL-ImG.

Assumption 2. *Decentralized controllers $\mathcal{C}_{[i]}$, $i \in \mathcal{D}$ are designed such that* (19) *holds with*

$$P_i = \left(\begin{array}{c|cc} \eta_i & 0 & 0 \\ \hline 0 & \bullet & \bullet \\ 0 & \bullet & \bullet \end{array}\right) \tag{22}$$

where $\bullet$ denotes an arbitrary entry and $\eta_i > 0$ is a local parameter.

As regards Assumption 2, we will show later that checking the existence of P_i as in (22) and K_i fulfilling (19) leads to solving a convex optimization problem.

The next Proposition provides the main stability result.

Proposition 3. *There exist $\eta_i > 0$, $i = 1, \dots, N$ such that, under Assumption 2, the overall closed-loop QSL-ImG is asymptotically stable.*

Proof. We have to show that (21) holds, which is equivalent to prove that

$$\underbrace{(\hat{\mathbf{A}}_\mathbf{D} + \hat{\mathbf{B}}\mathbf{K})^T\mathbf{P} + \mathbf{P}(\hat{\mathbf{A}}_\mathbf{D} + \hat{\mathbf{B}}\mathbf{K})}_{(a)} + \underbrace{\hat{\mathbf{A}}_\mathbf{C}^T\mathbf{P} + \mathbf{P}\hat{\mathbf{A}}_\mathbf{C}}_{(b)} < 0. \tag{23}$$

We highlight that term (a) is a block diagonal matrix that collects on its diagonal all left-hand sides of (19). It follows that term (a) is a negative definite matrix. Moreover, each block (i,j) of term (b) can be written as

$$\begin{cases} P_i\hat{A}_{ij} + \hat{A}_{ji}^T P_j & \text{if } j \in \mathcal{N}_i \\ 0 & \text{otherwise} \end{cases}$$

where

$$P_i\hat{A}_{ij} = \begin{pmatrix} \frac{\eta_i}{R_{ij}C_{ti}} & 0 & 0 \\ 0 & 0 & 0 \\ 0 & 0 & 0 \end{pmatrix} \text{ and } \hat{A}_{ji}^T P_j = \begin{pmatrix} \frac{\eta_j}{R_{ji}C_{tj}} & 0 & 0 \\ 0 & 0 & 0 \\ 0 & 0 & 0 \end{pmatrix}.$$

It turns out that term (b) can be made arbitrarily close to zero by setting coefficients η_i small enough. In view of the fact that term (a) is negative definite, there always exist coefficients η_i guaranteeing that (23) is fulfilled. □

The proof of Proposition 3 highlights that coefficients η_i, which are tuning knobs that can be set by the user, should be chosen such that $\frac{\eta_i}{R_{ij}C_{ti}} \approx 0$, $\forall i \in \mathcal{D}$, $\forall j \in \mathcal{N}_i$. Furthermore, controllers K_i should be designed such that inequality

$$(\hat{A}_{ii} + \hat{B}_i K_i)^T P_i + P_i(\hat{A}_{ii} + \hat{B}_i K_i) + \gamma_i^{-1} I \leq 0 \tag{24}$$

is fulfulled for $\gamma_i > 0$ large enough and matrix P_i structured as in (22). In order to complete the design of the local controller $\mathcal{C}_{[i]}$, we have to solve the following problem.

Problem 1. *Compute a vector K_i such that the nominal closed-loop subsystem is asymptotically stable and Assumption 2 is verified, i.e.* (19) *holds for a matrix P_i structured as in* (22)*.*

Consider the following optimization problem

$$\begin{aligned} \mathcal{O}_i : \min_{Y_i, G_i, \gamma_i, \beta_i, \delta_i} \quad & \alpha_{i1}\gamma_i + \alpha_{i2}\beta_i + \alpha_{i3}\delta_i \\ & Y_i = \begin{bmatrix} \eta_i^{-1} & 0 & 0 \\ 0 & \bullet & \bullet \\ 0 & \bullet & \bullet \end{bmatrix} > 0 && \text{(25a)} \\ & \begin{bmatrix} Y_i\hat{A}_{ii}^T + G_i^T\hat{B}_i^T + \hat{A}_{ii}Y_i + \hat{B}_i G_i & Y_i \\ Y_i & -\gamma_i I \end{bmatrix} \leq 0 && \text{(25b)} \\ & \begin{bmatrix} -\beta_i I & G_i^T \\ G_i & -I \end{bmatrix} < 0 && \text{(25c)} \\ & \begin{bmatrix} Y_i & I \\ I & \delta_i I \end{bmatrix} > 0 && \text{(25d)} \\ & \gamma_i > 0, \quad \beta_i > 0, \quad \delta_i > 0 && \text{(25e)} \end{aligned}$$

where α_{i1}, α_{i2} and α_{i3} represent positive weights and $\bullet$ are arbitrary entries. Since all constraints in (25) are Linear Matrix Inequalities (LMI), the optimization problem is convex and can be solved with efficient (i.e. polynomial-time) LMI solvers [36].

Lemma 1. *Problem $\mathcal{O}_i$ is feasible if and only if Problem 1 has a solution. Moreover, K_i and P_i in* (19) *are given by $K_i = G_i Y_i^{-1}$, $P_i = Y_i^{-1}$ and*

$$||K_i||_2 < \sqrt{\beta_i}\delta_i. \tag{26}$$

Proof. Inequality (19) is equivalent to the existence of $\gamma_i > 0$ such that (24) holds. By applying the Schur lemma on (24), we get the following inequality

$$\begin{bmatrix} (\hat{A}_{ii} + \hat{B}_i K_i)^T P_i + P_i(\hat{A}_{ii} + \hat{B}_i K_i) & I \\ I & -\gamma_i I \end{bmatrix} \leq 0 \tag{27}$$

which is nonlinear in P_i and K_i. In order to get rid of the nonlinear terms, we perform the following parametrization trick [36]

$$\begin{aligned} Y_i &= P_i^{-1} \\ G_i &= K_i Y_i. \end{aligned} \tag{28}$$

Notice that the structure of Y_i is the same as the structure of P_i. By pre- and post-multiplying (27) with $\left[\begin{smallmatrix} Y_i & 0 \\ 0 & I \end{smallmatrix}\right]$ and exploiting (28) we obtain

$$\begin{bmatrix} Y_i\hat{A}_{ii}^T + G_i^T\hat{B}_i^T + \hat{A}_{ii}Y_i + \hat{B}_i G_i & Y_i \\ Y_i & -\gamma_i I \end{bmatrix} \leq 0 \tag{29}$$

Constraint (25a) ensures that matrix P_i has the structure required by Assumption 2. At the same time, constraint (25b) guarantees stability of the closed-loop subsystem. Further constraints appear in Problem $\mathcal{O}_i$ with the aim of bounding $||K_i||_2$. In particular, we add $||G_i||_2 < \sqrt{\beta_i}$ and $||Y_i^{-1}||_2 < \delta_i$ (which, via Schur complement, correspond to constraints (25c) and (25d)) to prevent $||K_i||_2$ from becoming too large. These bounds imply $||K_i||_2 < \sqrt{\beta_i}\delta_i$ and then affect the magnitude of control variables. □

Remark 3. *From* (24)*, the parameter γ_i is the inverse of the quadratic stability margin [36], which is a measure of robust stability. Furthermore, from* (26)*, small β_i and δ_i prevent the control action from becoming too aggressive. A suitable tuning of weights α_{i1}, α_{i2} and α_{i3} in the cost of problem $\mathcal{O}_i$ allows one to achieve a balance between these performance requirements.*

Next, we discuss the key feature of the proposed decentralized control approach. We first notice that constraints in (25) depend upon local fixed matrices ($\hat{A}_{ii}$, $\hat{B}_i$) and local design parameters (α_{i1}, α_{i2}, α_{i3}). It follows that the computation of controller $\mathcal{C}_{[i]}$ is completely independent from the computation of controllers $\mathcal{C}_{[j]}$ when $j \neq i$ since, provided that problem $\mathcal{O}_i$ is feasible, controller $\mathcal{C}_{[i]}$ can be directly obtained through $K_i = G_i Y_i^{-1}$. In addition, it is clear that constraints (25c) and (25d) affect only the magnitude of control variables as stated in Lemma 1. Finally, if problems $\mathcal{O}_i$ are feasible for sufficiently small coefficients η_i, all assumptions in Proposition 3 can be verified, thus obtaining that the overall closed-loop QSL-ImG is asymptotically stable.

Remark 4. *The two main source of conservativeness of our approach are the block-diagonal structure of the Lyapunov matrix* $\mathbf{P}$ *and the structure* (22) *of matrices* P_i*. The former assumption is common in decentralized control [28] and it is mild because, as shown in the proof of Proposition 3, DGUs interactions have little impact on the fulfillment of* (21) *for sufficiently small* η_i*.*
Requiring that the stability of each DGU $\Sigma_{[i]}^{DGU}$ *can be certified through the Lyapunov function* $\mathcal{V}_{[i]}(x_{[i]}) = x_{[i]}^T P_i x_{[i]}$*, with* P_i *as in* (22)*, is more critical. Indeed,* (22) *requires that* $\mathcal{V}_{[i]}$ *is separable, i.e.* $\mathcal{V}_{[i]} = \eta_i V_i^2 + \tilde{\mathcal{V}}(I_{ti}, v_i)$*, for a suitable function* $\tilde{\mathcal{V}}(I_{ti}, v_i)$*. This suggests to look at the closed-loop dynamics of* $\hat{\Sigma}_{[i]}^{DGU}$ *as the interaction of two subsystems with state* V_i *and* $[I_{ti}, v_i]^T$*, respectively. Letting* $K_i = [k_{i1}, k_{i2}, k_{i3}]$*, the matrix* $\hat{A}_i + \hat{B}_i K_i$ *can be partitioned as*

$$\hat{A}_i + \hat{B}_i K_i = \left[\begin{array}{c|cc} \sum\limits_{j\in\mathcal{N}_i} -\frac{1}{R_{ij}C_{ti}} & \frac{1}{C_{ti}} & 0 \\ \hline \frac{k_{i1}-1}{L_{ti}} & \frac{k_{i2}-R_{ti}}{L_{ti}} & \frac{k_{i3}}{L_{ti}} \\ -1 & 0 & 0 \end{array}\right] = \left[\begin{array}{cc} \hat{A}_{cl,i1} & \hat{A}_{cl,i2} \\ \hat{A}_{cl,i3} & \hat{A}_{cl,i4} \end{array}\right].$$

Basic results in decentralized control [28] show that the possibility of certifying stability of $\hat{A}_i + \hat{B}_i K_i$ *through* $\mathcal{V}_{[i]}$ *(i.e. the fulfillment of (21)) depends on the magnitude of the interconnection terms* $\hat{A}_{cl,i2}$ *and* $\hat{A}_{cl,i3}$ *(if they were both zero, the structure* (22) *would not be conservative). Note also that the local controller can partially modify* $\hat{A}_{cl,i3}$ *but not* $\hat{A}_{cl,i2}$*.*

C. QSL approximations as singular perturbations

We now discuss stability properties brought about by our controllers when applied to the ImG model obtained without using QSL approximations. In other words, from (1a)-(1c), (12) and (17), we study stability of the closed-loop ImG given by the controlled DGU models

$$\dot{\hat{x}}_{[i]}(t) = \hat{A}_i^\circ \hat{x}_{[i]} + \hat{M}_i \hat{d}_{[i]} + \left[\begin{array}{c} \frac{1}{C_{ti}} \sum_{j\in\mathcal{N}_i} I_{ij} \\ 0 \\ 0 \end{array}\right], \quad i \in \mathcal{D} \tag{30}$$

$$\hat{A}_i^\circ = \left[\begin{array}{ccc} 0 & \frac{1}{C_{ti}} & 0 \\ \frac{k_{i1}-1}{L_{ti}} & \frac{k_{i2}-R_{ti}}{L_{ti}} & \frac{k_{i3}}{L_{ti}} \\ -1 & 0 & 0 \end{array}\right]$$

and the line dynamics (1c), i.e.

$$L_{ij}\dot{I}_{ij} = -R_{ij}I_{ij} + [1\ 0\ 0](\hat{x}_{[j]} - \hat{x}_{[i]}), \quad \forall (i,j) \in \mathcal{E} \tag{31}$$

Theorem 1. *If the closed-loop QSL-ImG is asymptotically stable, then there is* $\bar{\varepsilon} > 0$ *such that, if* $L_{ij} < \bar{\varepsilon}$*,* $\forall (i,j) \in \mathcal{E}$*, also the system* (30)-(31) *is asymptotically stable.*

Proof. The proof, that is based on results in [32], is reported in Appendix VI-B. □

D. Enhancements of local controllers for improving performances

In order to improve transient performances of controllers $\mathcal{C}_{[i]}$, we enhance them with feed-forward terms for
(i) pre-filtering reference signals;
(ii) compensating measurable disturbances.

1) Pre-filtering of the reference signal: Pre-filtering is a well known technique used to widen the bandwidth so as to speed up the response of the system. Consider the transfer function $F_{[i]}(s)$, from $z_{ref\,[i]}(t)$ to the controlled variable $z_{[i]}(t)$

$$F_{[i]}(s) = (\hat{H}_i \hat{C}_i)(sI - (\hat{A}_{ii} + \hat{B}_i K_i))^{-1} \begin{bmatrix} 0 \\ 1 \end{bmatrix} \tag{32}$$

of each nominal closed-loop subsystem (18). By virtue of a feedforward compensator $\tilde{C}_{[i]}(s)$, it is possible to filter the reference signal $z_{ref\,[i]}(t)$ (see Figure 3). Consequently, the

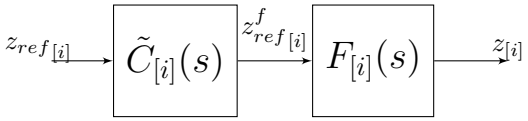

Fig. 3: Block diagram of closed-loop DGU i with prefilter.

new transfer function from $z_{ref\,[i]}(t)$ to $z_{[i]}(t)$ becomes

$$\tilde{F}_{[i]}(s) = \tilde{C}_{[i]}(s) F_{[i]}(s) \tag{33}$$

Now, taking a desired transfer function $\tilde{F}_{[i]}(s)$ for each subsystem, we can compute, from (33), the pre-filter $\tilde{C}_{[i]}(s)$ as

$$\tilde{C}_{[i]}(s) = \tilde{F}_{[i]}(s) F_{[i]}(s)^{-1} \tag{34}$$

under the following conditions [35]:
(PF1) $F_{[i]}(s)$ must not have Right-Half-Plane (RHP) zeros that would become RHP poles of $\tilde{C}_{[i]}(s)$, making it unstable;
(PF2) $F_{[i]}(s)$ must not contain a time delay, otherwise $\tilde{C}_{[i]}(s)$ would have a predictive action
(PF3) $\tilde{C}_{[i]}(s)$ must be realizable, i.e. it must have more poles than zeros.

Hence, if these conditions are fulfilled, the filter $\tilde{C}_{[i]}(s)$ given by (34) is realizable and asymptotically stable (this condition is essential since $\tilde{C}_{[i]}(s)$ works in open-loop). Furthermore, since $F_{[i]}(s)$ is asymptotically stable (controllers $\mathcal{C}_{[i]}$ are, in fact, designed solving the problem $\mathcal{O}_i$), the closed-loop system including filters $\tilde{C}_{[i]}(s)$ is asymptotically stable as well. We highlight that, if not all conditions (PF1), (PF2) and (PF3) are fulfilled, then expression (34) cannot be used. Still, the compensator $\tilde{C}_{[i]}(s)$ can be designed for being effective within a given bandwidth, as shown in [35].

2) Compensation of measurable disturbances: We remind that, since load dynamics is assumed to be unknown, we have modeled each load current as a measurable disturbance $d_{[i]}(t)$. Let us define new local controllers $\tilde{\mathcal{C}}_{[i]}$ as

$$\tilde{\mathcal{C}}_{[i]}: \quad u_{[i]} = K_i \hat{x}_{[i]}(t) + \tilde{u}_{[i]}(t) \tag{35}$$

Note that $\tilde{\mathcal{C}}_{[i]}$ are obtained by adding term $\tilde{u}_{[i]}(t)$ to the controllers $\mathcal{C}_{[i]}$ in (17). Hence, (18) can be rewritten as follows

$$\tilde{\Sigma}^{DGU}_{[i]}: \begin{cases} \dot{\hat{x}}_{[i]}(t) = (\hat{A}_{ii} + \hat{B}_i K_i)\hat{x}_{[i]}(t) + \hat{M}_i \hat{d}_{[i]}(t) + \hat{B}_i \tilde{u}_{[i]}(t) \\ \hat{y}_{[i]}(t) = \hat{C}_i \hat{x}_{[i]}(t) \\ z_{[i]}(t) = \hat{H}_i \hat{y}_{[i]}(t) \end{cases} \tag{36}$$

We now use the new input $\tilde{u}_{[i]}(t)$ to compensate the measurable disturbance $d_{[i]}(t)$ (recall that $\hat{d}_{[i]} = [d^T{}_{[i]} \; z^T_{ref\,[i]}]^T$). From (36), the transfer function from the disturbance $d_{[i]}(t)$ to the controlled variable $z_{[i]}(t)$ is

$$G^d_i(s) = (\hat{H}_i \hat{C}_i)(sI - (\hat{A}_{ii} + \hat{B}_i K_i))^{-1} \begin{bmatrix} M_i \\ 0 \end{bmatrix}. \tag{37}$$

Moreover, the transfer function from the new input $\tilde{u}_{[i]}(t)$ to the controlled variable $z_{[i]}(t)$ is

$$G_i(s) = (\hat{H}_i \hat{C}_i)(sI - (\hat{A}_{ii} + \hat{B}_i K_i))^{-1} \hat{B}_i. \tag{38}$$

If we combine (37) and (38), we obtain

$$z_{[i]}(s) = G_i(s)\tilde{u}_{[i]}(s) + G^d_i(s) d_{[i]}(s). \tag{39}$$

In order to zero the effect of the disturbance on the controlled variable, we set

$$\tilde{u}_{[i]}(s) = N_i(s) d_{[i]}(s),$$

where

$$N_{[i]}(s) = -G_i(s)^{-1} G^d_i(s) \tag{40}$$

is the transfer function of the compensator. Note that $N_{[i]}(s)$ is well defined under the following conditions [35]:

- (C1) $G_{[i]}(s)$ must not have RHP zeros that would become RHP poles of $N_{[i]}(s)$;
- (C2) $G_{[i]}(s)$ must not contain a time delay, otherwise $N_{[i]}(s)$ would have a predictive action
- (C3) $N_{[i]}(s)$ must be realizable, i.e. it must have more poles than zeros.

In this way, we can ensure that the compensator $N_{[i]}(s)$ is asymptotically stable, hence preserving asymptotic stability of the system. When not all conditions (C1), (C2) and (C3) are fulfilled, formula (40) cannot be used and perfect compensation cannot be achieved. Still, the compensator $N_{[i]}(s)$ can be designed to reject disturbances within a given bandwidth, as shown in [35]. The overall control scheme with the addition of the compensators is shown in Figure 4.

E. Algorithm for the design of local controllers

Algorithm 1 collects the steps of the overall design procedure.

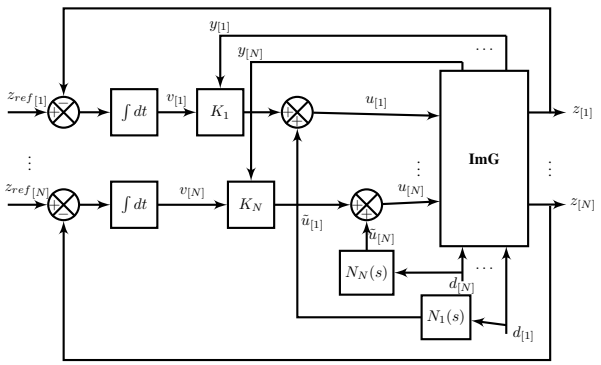

Fig. 4: Overall microgrid control scheme with compensation of measurable disturbances $d_{[i]}(s)$.

Algorithm 1 Design of controller $\mathcal{C}_{[i]}$ and compensators $\tilde{C}_{[i]}$ and $N_{[i]}$ for subsystem $\hat{\Sigma}^{DGU}_{[i]}$

Input: DGU $\hat{\Sigma}^{DGU}_{[i]}$ as in (13)

Output: Controller $\mathcal{C}_{[i]}$ and, optionally, pre-filter $\tilde{C}_{[i]}$ and compensator $N_{[i]}$

(A) Find K_i solving the LMI problem (25). If it is not feasible **stop** (the controller $\mathcal{C}_{[i]}$ cannot be designed).
Optional steps
(B) Design the asymptotically stable local pre-filter $\tilde{C}_{[i]}$ and compensator $N_{[i]}$ as in (40).

F. PnP operations

In the following section, the operations for updating the controllers when DGUs are added to or removed from an ImG are discussed. We remind that all these operations are performed with the aim of preserving stability of the new closed-loop system. Consider, as a starting point, a microgrid composed of subsystems $\hat{\Sigma}^{DGU}_{[i]}, i \in \mathcal{D}$ equipped with local controllers $\mathcal{C}_{[i]}$ and compensators $\tilde{C}_{[i]}$ and $N_{[i]}$, $i \in \mathcal{D}$ produced by Algorithm 1.

Plugging-in operation Assume that the plug-in of a new DGU $\hat{\Sigma}^{DGU}_{[N+1]}$ described by matrices, $\hat{A}_{N+1\,N+1}$, $\hat{B}_{N+1}$, $\hat{C}_{N+1}$, $\hat{M}_{N+1}$, $\hat{H}_{N+1}$ and $\{\hat{A}_{N+1\,j}\}_{j\in\mathcal{N}_{N+1}}$ needs to be performed. Let $\mathcal{N}_{N+1}$ be the set of DGUs that are directly coupled to $\hat{\Sigma}^{DGU}_{[N+1]}$ through power lines and let $\{\hat{A}_{N+1\,j}\}_{j\in\mathcal{N}_{N+1}}$ be the matrices containing the corresponding coupling terms. According to our method, the design of controller $\mathcal{C}_{[N+1]}$ and compensators $\tilde{C}_{[N+1]}$ and $N_{[N+i]}$ requires Algorithm 1 to be executed. Since DGUs $\hat{\Sigma}^{DGU}_{[j]}$, $j \in \mathcal{N}_{N+1}$, have the new neighbor $\hat{\Sigma}^{DGU}_{[N+1]}$, we need to redesign controllers $\mathcal{C}_{[j]}$ and compensators $\tilde{C}_{[j]}$ and $N_{[j]}$, $\forall j \in \mathcal{N}_{N+1}$ because matrices $\hat{A}_{jj}$, $j \in \mathcal{N}_{N+1}$ change.

Only if Algorithm 1 does not stop in Step (A) when computing controllers $\mathcal{C}_{[k]}$ for all $k \in \mathcal{N}_{N+1} \cup \{N+1\}$, we have that the plug-in of $\hat{\Sigma}^{DGU}_{[N+1]}$ is allowed. Moreover, we stress that the redesign is not propagated further in the network and therefore the asymptotic stability of the new overall closed-loop QSL-ImG model is preserved for a sufficient small

η_{N+1} even without changing controllers $\mathcal{C}_{[i]}$, $\tilde{C}_{[i]}$ and $N_{[i]}$, $i \notin \{N+1\} \cup \mathcal{N}_{N+1}$.

Unplugging operation Let us now examine the unplugging of DGU $\hat{\Sigma}_{[k]}^{DGU}$, $k \in \mathcal{D}$. The disconnection of $\hat{\Sigma}_{[k]}^{DGU}$ from the network leads to a change in matrix $\hat{A}_{jj}$ of each $\hat{\Sigma}_{[j]}^{DGU}$, $j \in \mathcal{N}_k$. Consequently, for each $j \in \mathcal{N}_k$, we have to redesign controllers $\mathcal{C}_{[j]}$ and compensators $\tilde{C}_{[j]}$ and $N_{[j]}$. As for the plug-in operation, we run Algorithm 1. If all operations can be successfully terminated, then the unplugging of $\hat{\Sigma}_{[k]}^{DGU}$ is allowed and stability is preserved without redesigning the local controllers $\mathcal{C}_{[j]}$, $j \notin \mathcal{N}_k$.

G. Hot plugging-in/-out operations

Plugging-in/-out operations can require to switch local controllers in real-time. In order to avoid jumps in the control variable at switching times, we embedded each local regulator into a bumpless control scheme [26] that is described in Appendix VI-A.

In particular, prior to real-time plugging-in operation (*hot plugging-in*), it is recommended to keep set points constant for a sufficient amount of time so as to guarantee the control variable in the bumpless control scheme is in steady state. This ensures smooth behaviors of the electrical variables. Similarly, when an unplugging operation is scheduled in advance, it is advisable to follow an *hot unplugging* protocol similar to the one described above for plugging-in.

IV. Simulation results

In this section, we study performance due to PnP controllers described in Section III. As a starting point, we consider the ImG depicted in Figure 1 with only two DGUs (Scenario 1) and we evaluate performance in terms of (i) tracking step references, (ii) transients after the hot plugging-in of the two DGUs and (iii) robustness to unknown load dynamics. Then, we extend the analysis to an ImG with 6 DGUs (Scenario 2) and we show that stability of the whole microgrid is guaranteed.

Simulations have been performed in PSCAD, a simulation environment for electric systems that allows to implement the ImG model with realistic electric components.

A. Scenario 1

In this Scenario, we consider the ImG shown in Figure 1 composed of two identical DC DGUs connected through RL lines supporting 10 Ω and 6 Ω loads, respectively. The duration of the simulation is 8 seconds and, for the sake of simplicity, we set $i = 1$ and $j = 2$. The output voltage reference has been selected at $48\ V$ and it is equal for both DGUs. Parameters values for all DGUs are given in Table I. Notice that that they are comparable to those used in [25]. Figures 6 and 7 show the voltages at PCC_1 and PCC_2, respectively, for the whole simulation.

Parameter	Symbol	Value
DC power supply	V_{DC}	$100\ V$
Output capacitance	C_{t*}	$2.2\ m$F
Converter inductance	L_{t*}	$1.8\ m$H
Inductor + switch loss resistance	R_{t*}	$0.2\ \Omega$
Switching frequency	f_{sw}	10 kHz
Power line inductance	L_{12}	$1.8\ \mu$H
Power line resistance	R_{12}	$0.05\ \Omega$

TABLE I: Electrical setup of DGU $* \in \{1, 2\}$ and line parameters in Scenario 1.

1) Voltage reference tracking at the startup: We assume that at the beginning of the simulation ($t = 0$ s), subsystems $\hat{\Sigma}_{[1]}^{DGU}$ and $\hat{\Sigma}_{[2]}^{DGU}$ are not interconnected. Therefore, stabilizing controllers $\mathcal{C}_i$, $i = 1, 2$ are designed neglecting coupling among DGUs. Moreover, in order to widen the bandwidth of each closed-loop subsystem, we use local pre-filters $\tilde{C}_{[i]}$, $i = 1, 2$ of reference signals. The desired closed-loop transfer functions $\tilde{F}_i(s)$, $i = 1, 2$ have been chosen as low-pass filters with DC gain equal to 0 dB and bandwidth equal to 100 Hz. The eigenvalues of the two decoupled closed-loop QSL subsystems are shown in Figure 5a. Moreover, by running Step (B) of Algorithm 1 we obtain two asymptotically stable local pre-filters $\tilde{C}_i$, $i = 1, 2$ whose Bode magnitude plots are depicted in Figure 5b. Notice that through the addition of the pre-filters, the frequency response of the two closed-loop transfer functions $F_i(s)$, $i = 1, 2$ coincide with the frequency response of the desired transfer functions $\tilde{F}_i(s)$, $i = 1, 2$ (see the green line in Figure 5c). From Figures 6 and 7 we notice

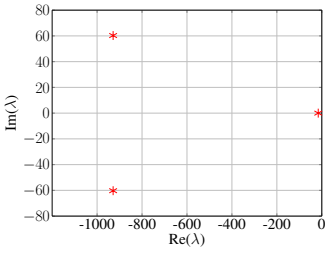

(a) Eigenvalues of each of the two decoupled closed-loop QSL subsystems.

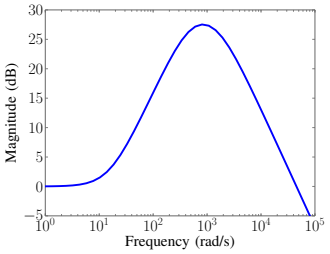

(b) Bode magnitude plot of pre-filters $\tilde{C}_{[i]}(s)$, $i = 1, 2$.

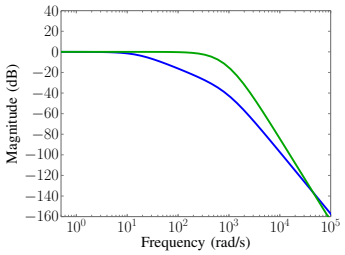

(c) Bode magnitude plot of $F_i(s)$, $i = 1, 2$ with (green) and without (blue) pre-filters.

Fig. 5: Features of PnP controllers for Scenario 1 when the DGUs are not interconnected.

that, at startup, the controllers ensure excellent tracking of the reference signals in a very short time (both voltages at PCC_1 and PCC_2 are equal to zero at $t = 0$).

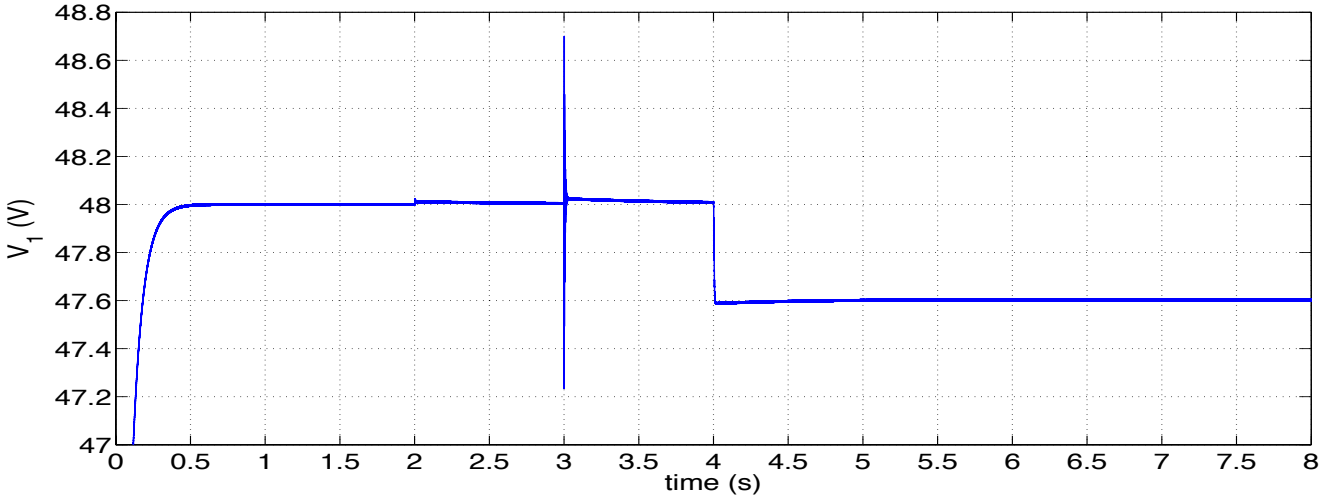

Fig. 6: Scenario 1 - Voltage at PCC_1.

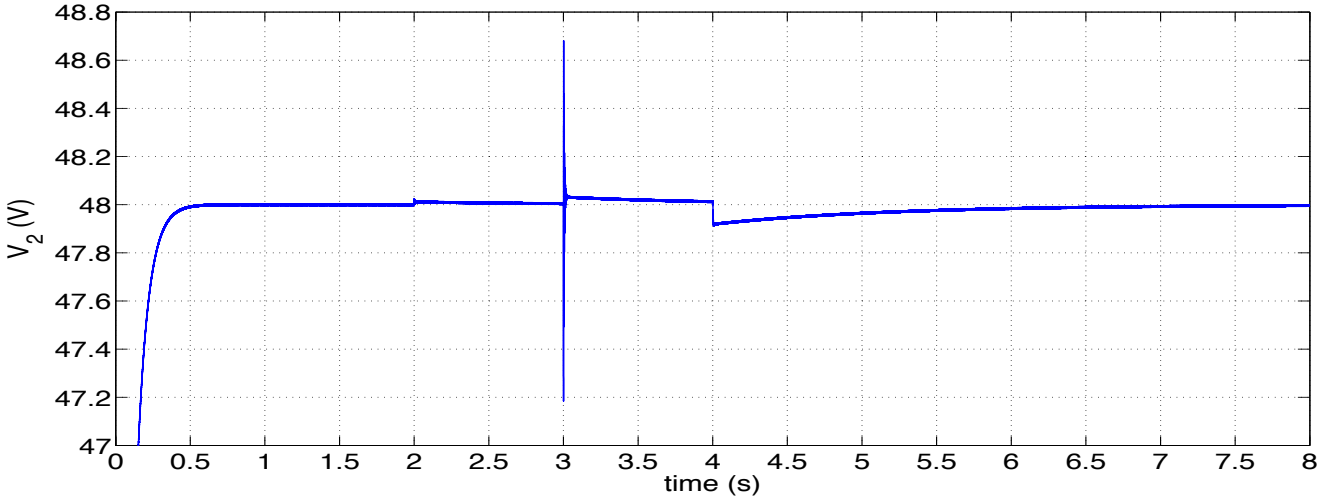

Fig. 7: Scenario 1 - Voltage at PCC_2.

2) Hot plugging-in of DGUs 1 and 2: At time $t = 2$ s, we connect DGUs 1 and 2 together. This requires real-time switching of the local controllers which translates into two hot plugging-in operations, as described in Section III-G. The new decentralized controllers for subsystems $\hat{\Sigma}^{DGU}_{[1]}$ and $\hat{\Sigma}^{DGU}_{[2]}$ are designed running Algorithm 1. As shown in Section III-F, the interconnection of the two subsystems leads to a variation of each DGU dynamics, therefore even compensators $\tilde{C}_{[i]}$ and $N_{[i]}$, $i = 1, 2$ need to be updated. In particular, the new desired closed-loop transfer functions $\tilde{F}_i(s)$, $i = 1, 2$ have been chosen as low-pass filters with DC gain equal to 0 dB and bandwidth equal to 100 Hz.

Since Algorithm 1 never stops in Step (A), the hot plug-in of the DGUs is allowed and local controllers get replaced by the new ones at $t = 2$ s. Figure 8a shows the closed-loop eigenvalues of the overall QSL ImG composed of two interconnected DGUs. The Bode magnitude plots of compensators $\tilde{C}_{[i]}$ and $N_{[i]}$, $i = 1, 2$ are depicted in Figure 8b and 8c, respectively, while the singular values of the overall closed-loop transfer function $F(s)$ with inputs $[z_{ref_{[1]}}, z_{ref_{[2]}}]^T$ and outputs $[z_{[1]}, z_{[2]}]^T$ are shown in Figure 8d.

Figures 6 and 7 show that bumpless control transfer schemes ensure no significant deviations in the output signals when the controller switch is performed at $t = 2$ s.

3) Robustness to unknown load dynamics: Next, we assess the performance of PnP controllers when loads suddenly change. To this purpose, at $t = 3$ s we decrease the load resistances at PCC_1 and PCC_2 to half of their initial values. Oscillations visible in Figures 6 and 7 are zoomed out in Figures 9a and 9b, respectively. These plots confirm very good compensation of the current disturbances produced by load changes. The small oscillations of the voltage signals are due to the presence of complex conjugate poles in the transfer function of the overall closed-loop microgrid including couplings (as shown in Figure 8a). However, these oscillations disappear after a short transient. We recall that load currents

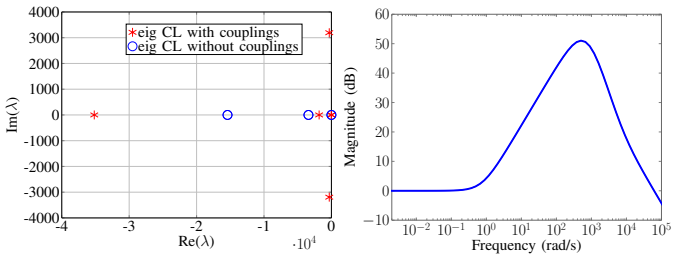

(a) Eigenvalues of the closed-loop QSL microgrid with (stars) and without (circles) couplings.

(b) Bode magnitude plot of pre-filters $\tilde{C}_{[i]}(s)$, $i = 1, 2$.

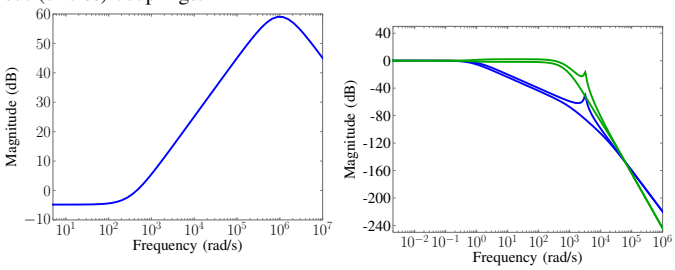

(c) Bode magnitude plot of disturbances compensators $N_{[i]}(s)$, $i = 1, 2$.

(d) Singular values of $F(s)$ with (green) and without (blue) pre-filters.

Fig. 8: Features of PnP controllers for Scenario 1 when the DGUs are connected together.

(see Figures 9c and 9d) are treated as measurable disturbances in our model, and a variation of the load resistance induces step-like changes in the disturbances.

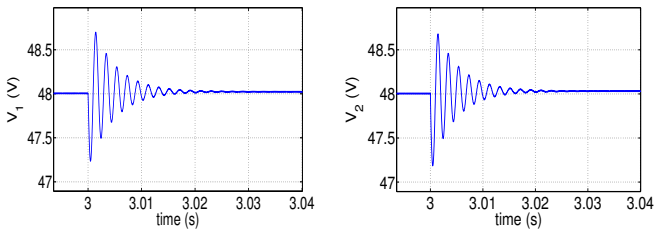

(a) Voltage at PCC_1.

(b) Voltage at PCC_2.

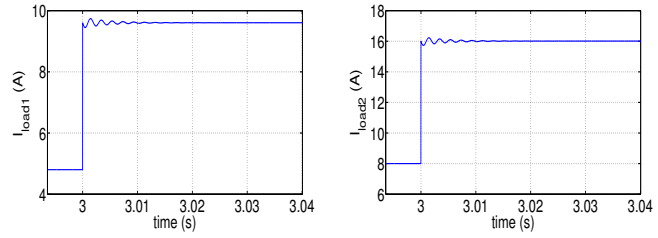

(c) Instantaneous load current I_{L1}.

(d) Instantaneous load current I_{L2}.

Fig. 9: Scenario 1 - Performance of PnP decentralized voltage control in presence of load switches at time $t = 3$ s.

4) Voltage tracking for DGU 1: Finally, we evaluate the performance in tracking step changes in the voltage reference at one PCC (e.g. PCC_1) when the DGUs are connected together. This test is of particular concern if we look at the concrete implementation of islanded DC microgrids. In fact, changes in the voltage references can be required in order to regulate power flow among the DGUs, or to control the state-of-charge of batteries possibly embedded in the ImG.

To this purpose, at $t = 4$ s we let the reference signal of DGU 1, $v^{\star}_{1,MG}$, step down to $47.6\ V$. Notice that this small variation of the voltage reference at PCC_1 is sufficient to let an appreciable amount of current flow through the line, since the line impedance is quite small. Figure 6 shows how PnP controllers are capable to guarantee good tracking performances for DGU 1, when the corresponding voltage reference is changed ($t = 4$ s). Moreover, interactions between the two DGUs are small (see Figure 7).

B. Scenario 2

In this second scenario, we consider the meshed ImG shown in black in Figure 11 and composed by 5 DGUs. Differently from Scenario 1, some DGUs have more than one neighbor. This means that the disturbances influencing their dynamics will be greater. Moreover, the presence of a loop further complicates voltage regulation. To our knowledge, control of loop-interconnected DGUs has never been attempted for DC microgrids.

In order to assess the capability of the proposed decentralized approach to cope with heterogeneous dynamics, we consider an ImG composed of DGUs with non-identical electrical parameters. They are listed in Tables 2, 3 and 4 in Appendix C of [29]. In order to allow for current flow through the lines, we set slightly different voltage references for the DGUs composing the ImG in Figure 11 (see Table II). We also assume that DGUs 1-5 supply 10 Ω, 6 Ω, 4 Ω, 2 Ω and 3 Ω loads, respectively. Moreover, we highlight that, for this Scenario, no compensators $\tilde{C}_i$ and N_i have been used. The duration of the simulation is 15 seconds. At $t = 0$, all the DGUs are assumed to be isolated and not connected to each other. However, we choose to equip each subsystem $\hat{\Sigma}^{DGU}_{[i]}$, $i \in \mathcal{D} = \{1, \ldots, 5\}$, with controller $\mathcal{C}_{[i]}$ designed by running Algorithm 1 and taking into account couplings among DGUs. This is possible because, as shown in Section III-B, local controllers stabilize the ImG also in absence of couplings. Because of this choice of local controllers in the startup phase, when the five subsystems are connected together at time $t = 1.5$ s, no bumpless control scheme is required since no real-time switch of controllers is performed. The closed-loop eigenvalues of the overall QSL ImG are depicted in Figure 10a while Figure 10b shows the closed-loop transfer function of the whole microgrid.

DGU	Voltage reference (V)
$\hat{\Sigma}^{DGU}_{[1]}$	47.9
$\hat{\Sigma}^{DGU}_{[2]}$	48
$\hat{\Sigma}^{DGU}_{[3]}$	47.7
$\hat{\Sigma}^{DGU}_{[4]}$	48
$\hat{\Sigma}^{DGU}_{[5]}$	47.8
$\hat{\Sigma}^{DGU}_{[6]}$	48.1

TABLE II: Scenario 2 - Voltage references for DGUs $\hat{\Sigma}^{DGU}_{[i]}$, $i = \{1, \ldots, 6\}$.

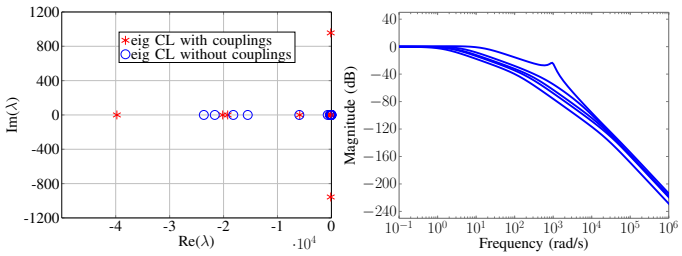

(a) Eigenvalues of the closed-loop QSL microgrid with (stars) and without (circles) couplings.

(b) Singular values of $F(s)$.

Fig. 10: Features of PnP controllers for Scenario 2 with 5 interconnected DGUs.

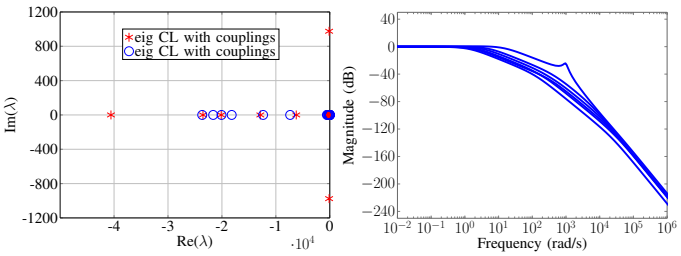

(a) Eigenvalues of the closed-loop QSL microgrid with (stars) and without (circles) couplings.

(b) Singular values of $F(s)$.

Fig. 12: Features of PnP controllers for Scenario 2 with 6 interconnected DGUs

1) Plug-in of a new DGU: For evaluating the PnP capabilities of our control approach, at time $t = 4$ s, we simulate the connection of DGU $\hat{\Sigma}^{DGU}_{[6]}$ with $\hat{\Sigma}^{DGU}_{[1]}$ and $\hat{\Sigma}^{DGU}_{[5]}$, as shown in Figure 11. This requires real-time updating of the

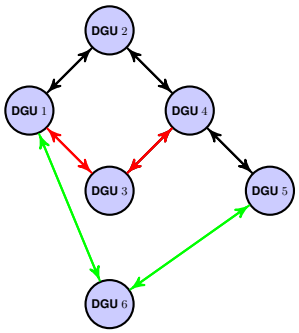

Fig. 11: Scenario 2 - Scheme of the ImG composed of DGUs 1-5 until $t = 4$ s and of 6 DGUs after the plugging-in of $\hat{\Sigma}^{DGU}_{[6]}$ (in green). At time $t = 12$ s, DGU 3 is removed (in red).

controllers $\mathcal{C}_{[j]}$, $j \in \mathcal{N}_6$, with $\mathcal{N}_6 = \{1, 5\}$ (see Section III-F). Notably, the new controllers for subsystems $\hat{\Sigma}^{DGU}_{[1]}$, $\hat{\Sigma}^{DGU}_{[5]}$ and $\hat{\Sigma}^{DGU}_{[5]}$ are synthesized running Algorithm 1 and, since it never stops in Step (A), the hot plug-in of DGU 6 is allowed. At the same time, the local regulators for DGU 1 and 5 get replaced by the new ones at $t = 4$ s. Figures 12a and 12b show, respectively, the closed-loop eigenvalues and the singular values of the closed-loop $F(s)$ of the overall QSL ImG represented in Figure 11 and equipped with the controllers described above. Moreover, from Figure 13, we note that, despite of the different voltages at PCCs of DGUs 1, 5 and 6, bumpless control transfer schemes ensure small deviations of the output signals from their references when controller switch is performed. Moreover, these perturbations disappear after short transients.

2) Robustness to unknown load dynamics: In order to test the robustness of the overall ImG to unknown load dynamics, at $t = 8$ s, the load of DGU 6 is decreased from 8 Ω to 4 Ω.

Figures 14a and 14b show that, when the load change of $\hat{\Sigma}^{DGU}_{[6]}$ occurs, the voltages at PCC_1 and PCC_5 exhibit very small variations which last for a short time. Then, load voltages of $\hat{\Sigma}^{DGU}_{[1]}$ and $\hat{\Sigma}^{DGU}_{[5]}$ converge to their reference

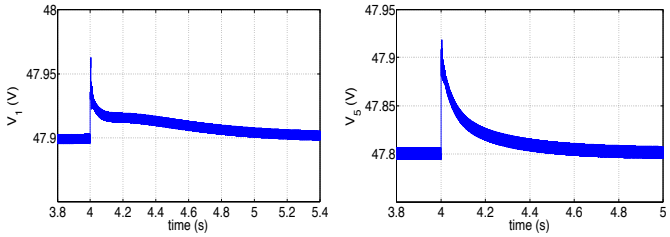

(a) Voltage at PCC_1.

(b) Voltage at PCC_5.

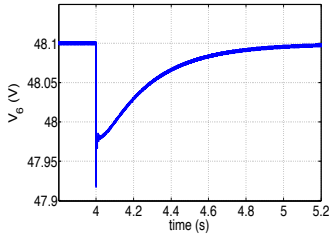

(c) Voltage at PCC_6.

Fig. 13: Scenario 2 - Performance of PnP decentralized voltage controllers during the hot plug-in of DGU 6 at time $t = 4$ s.

values. Similar remarks can be done for the new DGU $\hat{\Sigma}^{DGU}_{[6]}$: as shown in Figure 14c, there is a short transient at the time of the load change, that is effectively compensated by the control action. These experiments highlight that controllers $\mathcal{C}_{[i]}$, $i = 1, \ldots, 6$ may ensure very good tracking of the reference signal and robustness to unknown load dynamics even without using compensators $\tilde{C}_{[6]}$ and $N_{[6]}$.

3) Unplugging of a DGU: Next, we simulate the disconnection of $\hat{\Sigma}^{DGU}_{[3]}$ so that the considered ImG assumes the topology shown in Figure 11. The set of neighbors of DGU 3 is $\mathcal{N}_3 = \{1, 4\}$.

Because of the disconnection, there is a change in the local dynamics $\hat{A}_{jj}$ of DGUs $\hat{\Sigma}^{DGU}_{[j]}$, $j \in \mathcal{N}_3$. Then, each controller $\mathcal{C}_{[j]}$, $j \in \mathcal{N}_3$ must be redesigned (see Section III-F). Consequently, we run Algorithm 1 for computing the vectors K_1 and K_4 according to the new ImG topology. Since Algorithm 1 never stops in Step (A), the disconnection of $\hat{\Sigma}^{DGU}_{[3]}$ is allowed. Figure 15a shows that the closed-loop model of the new QSL microgrid is still asymptotically stable while Figure 15b shows the closed-loop transfer function $F(s)$ of the ImG. Hot-unplugging of $\hat{\Sigma}^{DGU}_{[3]}$ is performed

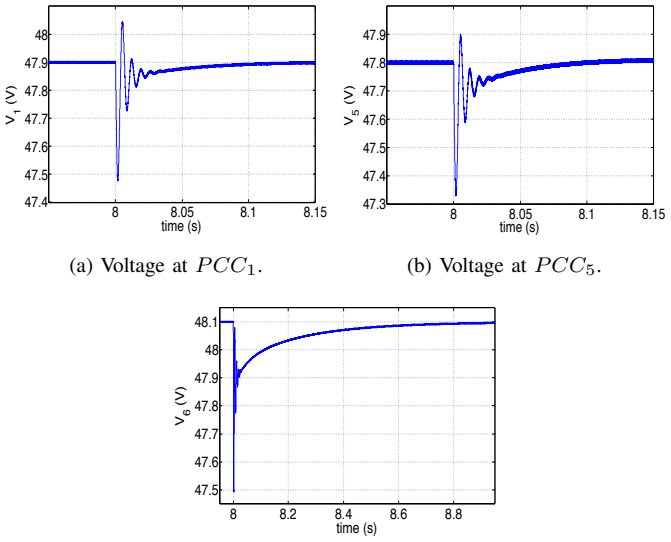

(a) Voltage at PCC_1. (b) Voltage at PCC_5.

(c) Voltage at PCC_6.

Fig. 14: Scenario 2 - Performance of PnP decentralized voltage controllers in terms of robustness to an abrupt change of load resistances at time $t = 8$ s.

at time $t = 12$ s. Even for the unplugging operation, by means of bumpless control transfer, load voltages of DGUs $\hat{\Sigma}^{DGU}_{[j]}$, $j \in \mathcal{N}_3$ show small deviation from their respective reference values when the hot-unplugging of DGU 3 (and, hence, updating of controllers $\mathcal{C}_{[1]}$ and $\mathcal{C}_{[5]}$) is performed at $t = 12$ s (see Figure 16). We stress again that stability of the microgrid is preserved despite the disconnection of $\hat{\Sigma}^{DGU}_{[3]}$.

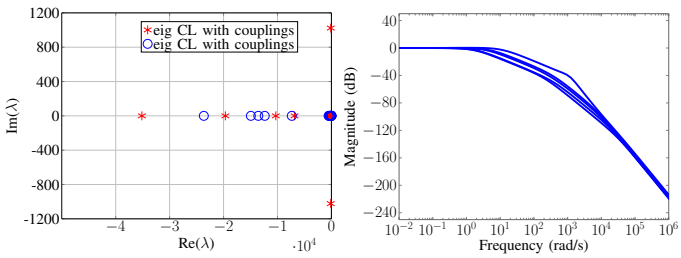

(a) Eigenvalues of the closed-loop QSL microgrid with (stars) and without (circles) couplings.

(b) Singular values of $F(s)$.

Fig. 15: Features of PnP controllers for Scenario 2 after the unplugging of DGU 3.

V. Conclusions

In this paper, a decentralized control scheme for guaranteeing voltage stability in DC ImGs was presented. The main feature of the proposed approach is that, whenever a plugging-in or -out of DGUs is required, only a limited number of local controllers must be updated. Moreover, as mentioned in Section IV-A4, local voltage controllers should be coupled with a higher control layer devoted to power flow regulation so as to orchestrate mutual help among DGUs. This can be done by letting the new control layer compute voltage set-points at PCCs. To this purpose, we will study if and how ideas from

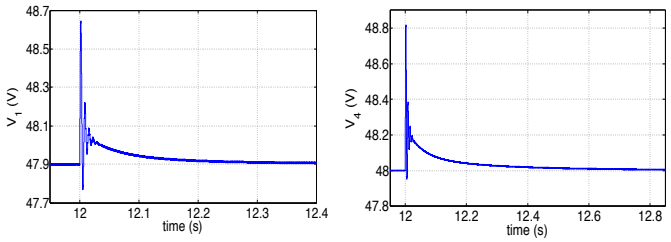

(a) Voltage at PCC_1. (b) Voltage at PCC_4.

Fig. 16: Scenario 2 - Performance of PnP decentralized voltage controllers during the hot-unplugging of DGU 3 at $t = 12$ s.

secondary control of ImGs [9], [21] can be reappraised in our context.

VI. Appendix

A. Bumpless control transfer

Since the controller $\mathcal{C}_{[i]}$ and the compensators $\tilde{C}_{[i]}$ and $N_{[i]}$ are dynamic systems, it is necessary to make sure that their states are correctly initialized when a switch of the controller (i.e. a plugging-in or unplugging operation) is required. Assuming that the control switch is made at time $\bar{t}$, we call $u_{prec,i}$ the control signal produced by the controller $\mathcal{C}_{[i]}$ up to time $\bar{t}$. It might happen that the updated controller will provide a control variable $u_i(\bar{t})$ different from $u_{prec,i}(\bar{t})$. Therefore, it is necessary to ensure there is no substantial difference in the two values. This property is called *bumpless control transfer* and it has been first studied when switching between manual and PID control [26].

A bumpless control transfer implementation of PnP local controller for system $\hat{\Sigma}^{DGU}_{[i]}$ is illustrated in Figure 17.

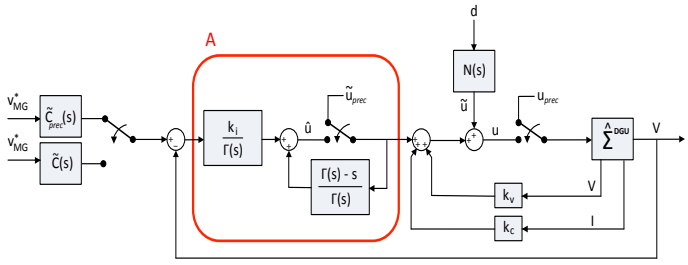

Fig. 17: Bumpless control transfer scheme. The three switches, close simultaneously at time $\bar{t}$

For the sake of simplicity, from now on, we drop the index i of the subsystem. Moreover, we assume all switches are in the position shown in Figure 17 at times $t < \bar{t}$ (so that the input $u^{prec}(t)$ is supplied to the system $\hat{\Sigma}^{DGU}$) and they close simultaneously at time $\bar{t}$ (hence providing the new input $u(t)$ to $\hat{\Sigma}^{DGU}$ from $t = \bar{t}$ on). The PnP controller activated at time $\bar{t}$ is given by

$$K = [k_v \;\; k_c \;\; k_i].$$

Notice that the integrator embedded in the DGU model for zeroing the steady-state error is replaced by block A (highlighted in red in Figure 17), where the polynomial $\Gamma(s)$ has

to be chosen such that $\frac{k_i}{\Gamma(0)} > 0$ and such that the transfer function

$$\Psi(s) = \frac{\Gamma(s) - s}{\Gamma(s)}$$

is asymptotically stable and realizable. Indeed, under these assumptions, the transfer function from the input to the output of block A is $\frac{k_i}{s}$ when the switch is closed.

In block A, a switch is present so that the signal is either $\tilde{u}_{prec}$ (up to time $\bar{t}$) or $\hat{u}$ (right after $\bar{t}$). The variable $\tilde{u}_{prec}$ is given by

$$\tilde{u}_{prec} = u_{prec} - k_v V - k_c I_t - \tilde{u} \tag{41}$$

where $\tilde{u}$ is the additional input produced by compensator $N(s)$, computed with respect to the dynamics of the system after the commutation ($N(s) = 0$ if such a compensation is not implemented). Notice that, choosing $\tilde{u}_{prec}$ as in (41) guarantees $u = u_{prec}$ right before the commutation. Moreover, we highlight that since there could be a transient in the $\hat{u}$ response to track signal $\tilde{u}_{prec}$, it is fundamental to wait for the two signals to become similar[3] before proceeding with the commutation. In this way we avoid jumps in the control variable.

Furthermore, if an optional prefilter of the reference is implemented, at time $\bar{t}$, it is also necessary to commute from transfer function $\tilde{C}_{prec}(s)$ to $\tilde{C}(s)$, since each plugging-in or unplugging operation of other DGUs in the overall ImG lead to a variation of the local dynamics of the considered subsystem $\hat{\Sigma}_i^{DGU}$ (see the term $\sum_{j\in\mathcal{N}_i} -\frac{1}{R_{ij}C_{ti}}$ in (7)).

B. Proof of Theorem 1

We treat each impedance L_{ij} in (31) as a singular perturbation parameter and exploit results in [32] on multiparameter singular perturbations. More specifically, we want to apply Theorem 5 in [32]. We denote with $\bar{N}$ the cardinality of $\mathcal{E}$, assign indexes $1, \dots, \bar{N}$ to pairs in $\mathcal{E}$, i.e. $\mathcal{E} = \{e_1, e_2, \dots, e_{\bar{N}}\}$, and define $\tilde{x} = [I_{e_1}, \dots, I_{e_{\bar{N}}}]^T$. Let also $\mathcal{I} \in \mathbb{R}^{|\mathcal{D}|\times\bar{N}}$ be the incidence matrix of the directed graph $\mathcal{G}$ with nodes $\mathcal{D}$ and edges $\mathcal{E}$. This means that, assuming $e_j = (k, \ell)$, row j of $\mathcal{I}$ has the elements

$$\mathcal{I} = \begin{cases} -1 & \text{if } i = k \\ 1 & \text{if } i = \ell \\ 0 & \text{otherwise} \end{cases}$$

By neglecting exogenous disturbances $\hat{d}_{[i]}$ in (30) (as they do not affect stability properties), model (30) and (31) can be written as

$$\dot{\hat{\mathbf{x}}} = \hat{\mathbf{A}}^\circ \hat{\mathbf{x}} + \hat{\mathbf{B}}^\circ \tilde{\mathbf{x}} \tag{42a}$$

$$\mathbf{E}(\varepsilon)\dot{\tilde{\mathbf{x}}} = \hat{\mathbf{C}}^\circ \hat{\mathbf{x}} + \hat{\mathbf{D}}^\circ \tilde{\mathbf{x}} \tag{42b}$$

where $\hat{\mathbf{A}}^\circ = \text{diag}(\hat{A}_1^\circ, \dots, \hat{A}_N^\circ)$, $\hat{\mathbf{B}}^\circ = \text{diag}(\hat{B}_1^\circ, \dots, \hat{B}_N^\circ)$, $\hat{\mathbf{C}}^\circ = \mathcal{I}^T \otimes [1\ 0\ 0]$, $\hat{\mathbf{D}}^\circ = \text{diag}(-R_{e_1}, \dots, -R_{e_{\bar{N}}})$, $\varepsilon = [L_{e_1}, \dots, L_{e_{\bar{N}}}]$ and $\mathbf{E}(\varepsilon) = \text{diag}(L_{e_1}, \dots, L_{e_{\bar{N}}})$.
In these matrices, L_e and R_e are the inductance and resistance of line $e \in \mathcal{E}$ (see (31)) and, from (30), blocks $\hat{B}_i^\circ$, $i, \dots, N$ are defined as

$$\hat{B}_i^\circ = \frac{1}{C_{ti}} \begin{bmatrix} 1_{\mathcal{N}_i} \\ 0_{\bar{N}} \\ 0_{\bar{N}} \end{bmatrix}$$

where $0_{\bar{N}}$ is a row vector composed by $\bar{N}$ zeros and the vector $1_{\mathcal{N}_i} \in \mathbb{R}^{1\times\bar{N}}$ has all zero entries, except those in positions $j \in \mathcal{N}_i$, which are equal to one.
We now verify assumptions of Theorem 5 in [32].
First, we check that matrix $\hat{\mathbf{D}}^\circ$ is strongly block D-stable relative to the multi index $(1, \dots, 1)$ made of $\bar{N}$ elements. From Definitions 1 and 3 in [32], characterizing strong block D-stability amounts to verify that there exists $\mu > 0$ such that, for all matrices $Q \in \mathbb{R}^{\bar{N}\times\bar{N}}$ verifying $||Q||_F = (\sum_{i=1}^{\bar{N}} \sum_{j=1}^{\bar{N}} (Q_{ij})^2)^{\frac{1}{2}} < \mu$ ($||\cdot||_F$ denotes the Frobenius norm) and for all $\theta_i > 0$, $i = 1, \dots, \bar{N}$, the matrices $\Theta(\hat{\mathbf{D}}^\circ + Q)$, $\Theta = \text{diag}(\theta_1, \dots, \theta_{\bar{N}})$ are Hurwitz (i.e. their eigenvalues have strictly negative real part).
To prove this property, we use the Gershgorin circle theorem [37]. Note that

$$\Theta(\hat{\mathbf{D}}^\circ + Q) = \begin{bmatrix} \theta_1(-R_{e_1} + Q_{11}) & \theta_1 Q_{12} & \dots & \theta_1 Q_{1\bar{N}} \\ \theta_2 Q_{21} & \theta_2(-R_{e_2} + Q_{22}) & \dots & \theta_2 Q_{2\bar{N}} \\ \vdots & \ddots & \ddots & 0 \\ \theta_{\bar{N}} Q_{\bar{N}1} & \theta_{\bar{N}} Q_{\bar{N}2} & \dots & \theta_{\bar{N}}(-R_{e_{\bar{N}}} + Q_{\bar{N}\bar{N}}) \end{bmatrix}.$$

Let $\mathcal{B}(c, \rho) \subset \mathbb{C}$ be the closed ball of center c and radius ρ. Then, all eigenvalues of $\Theta(\hat{\mathbf{D}}^\circ + Q)$ are in the set $\bigcup_{i=1}^{\bar{N}} \mathcal{B}(c_i, \rho_i)$ where $c_i = \theta_i(-R_{e_i} + Q_{ii})$ and $\rho_i = \sum_{\substack{j=1 \\ j\neq i}}^{\bar{N}} |\theta_i Q_{ij}|$. Each ball $\mathcal{B}(c_i, \rho_i)$ collects only complex numbers with strictly negative real parts if

$$\theta_i(-R_{e_i} + Q_{ii}) < -\rho_i. \tag{43}$$

Since $\theta_i > 0$, condition (43) is equivalent to $\theta_i(-R_{e_i} + Q_{ii}) < \theta_i \sum_{\substack{j=1 \\ j\neq i}}^{\bar{N}} |Q_{ij}|$ and hence

$$\sum_{\substack{j=1 \\ j\neq i}}^{\bar{N}} |Q_{ij}| < R_{e_i} - Q_{ii}. \tag{44}$$

We show now that all conditions (44) for $i \in \mathcal{D}$ are fulfilled if $\mu = \frac{1}{\sqrt{\bar{N}}} \min_{e_i\in\mathcal{E}} R_{e_i}$. Indeed, if $\mu > ||Q||_F$, then

$$\min_{e_i\in\mathcal{E}} R_{e_i} > \sqrt{\bar{N}}||Q||_F \geq \sqrt{\bar{N}}||Q_{i,\bullet}||_2 \tag{45}$$

where $Q_{i,\bullet}$ is row i of matrix Q and $||Q_{i,\bullet}||_2 = (\sum_{j=1}^{\bar{N}} (Q_{i,j})^2)^{\frac{1}{2}}$ is its Euclidean norm. Denoting with $||Q_{i,\bullet}||_1 = \sum_{j=1}^{\bar{N}} |Q_{i,j}|$ the 1-norm of $Q_{i,\bullet}$, we have

$$\sqrt{\bar{N}}||Q_{i,\bullet}||_2 \geq ||Q_{i,\bullet}||_1 \geq Q_{ii} + \sum_{\substack{j=1 \\ j\neq i}}^{\bar{N}} |Q_{ij}|. \tag{46}$$

[3]This eventually happens because, by construction, $\Psi(s)$ is an asymptotically stable transfer function with unit gain.

From (45) and (46) we have

$$\min_{e_i \in \mathcal{E}} R_{e_i} - Q_{ii} > \sum_{\substack{j=1 \\ j \neq i}}^{\bar{N}} |Q_{ij}|.$$

that implies (44) for all $i \in \mathcal{D}$.

The last assumption of Theorem 5 in [32] that has to be verified is that the quasi-stationary model given by (42a) and

$$\hat{\mathbf{C}}^{\circ}\hat{\mathbf{x}} + \hat{\mathbf{D}}^{\circ}\tilde{\mathbf{x}} = 0 \tag{47}$$

is asymptotically stable, i.e. the matrix $\hat{\mathbf{A}}^{\circ} - \hat{\mathbf{B}}^{\circ}(\hat{\mathbf{D}}^{\circ})^{-1}\hat{\mathbf{C}}^{\circ}$ is Hurwitz. Note that (47) is the system of scalar equations

$$R_{e_j} I_{e_j} = V_{\ell} - V_k \quad \text{if } e_j = (k, \ell) \tag{48}$$

for all $e_j \in \mathcal{E}$.

Since (48) are the QSL conditions (3a), the model given by (42a) and (47) is the closed-loop QSL-ImG model, which is asymptotically stable by assumption. Then, the application of Theorem 5 of [32] completes the proof.

REFERENCES

[1] R. Lasseter, A. Akhil, C. Marnay, J. Stephens, J. Dagle, R. Guttromson, A. Meliopoulous, R. Yinger, and J. Eto, "The CERTS microgrid concept," *White paper for Transmission Reliability Program, Office of Power Technologies, US Department of Energy*, 2002.

[2] J. J. Justo, F. Mwasilu, J. Lee, and J.-W. Jung, "AC-microgrids versus DC-microgrids with distributed energy resources: A review," *Renewable and Sustainable Energy Reviews*, vol. 24, pp. 387–405, 2013.

[3] X. Liu, P. Wang, and P. C. Loh, "A hybrid ac/dc microgrid and its coordination control," *IEEE Transactions on Smart Grid*, vol. 2, no. 2, pp. 278–286, 2011.

[4] J. M. Guerrero, M. Chandorkar, T.-L. Lee, and P. C. Loh, "Advanced control architectures for intelligent microgrids - part I: decentralized and hierarchical control," *IEEE Transactions on Industrial Electronics*, vol. 60, no. 4, pp. 1254–1262, 2013.

[5] J. M. Guerrero, P. C. Loh, T.-L. Lee, and M. Chandorkar, "Advanced control architectures for intelligent microgrids - part II: Power quality, energy storage, and ac/dc microgrids," *IEEE Transactions on Industrial Electronics*, vol. 60, no. 4, pp. 1263–1270, 2013.

[6] S. Riverso, F. Sarzo, and G. Ferrari-Trecate, "Plug-and-play voltage and frequency control of islanded microgrids with meshed topology," *IEEE Transactions on Smart Grid*, vol. 6, no. 3, pp. 1176–1184, May 2015.

[7] S. Bolognani and S. Zampieri, "A distributed control strategy for reactive power compensation in smart microgrids," *IEEE Transactions on Automatic Control*, vol. 58, no. 11, pp. 2818–2833, 2013.

[8] A. Kwasinski, "Quantitative evaluation of DC microgrids availability: Effects of system architecture and converter topology design choices," *IEEE Transactions on Power Electronics*, vol. 26, no. 3, pp. 835–851, 2011.

[9] Q. Shafiee, T. Dragičević, J. C. Vasquez, and J. M. Guerrero, "Hierarchical Control for Multiple DC-Microgrids Clusters," *IEEE Transactions on Energy Conversion*, vol. 29, no. 4, pp. 922–933, 2014.

[10] A. T. Elsayed, A. A. Mohamed, and O. A. Mohammed, "DC microgrids and distribution systems: An overview," *Electric Power Systems Research*, vol. 119, pp. 407–417, 2015.

[11] J. W. Simpson-Porco, F. Dörfler, and F. Bullo, "Synchronization and power sharing for droop-controlled inverters in islanded microgrids," *Automatica*, vol. 49, no. 9, pp. 2603–2611, 2013.

[12] J. Schiffer, R. Ortega, A. Astolfi, J. Raisch, and T. Sezi, "Conditions for stability of droop-controlled inverter-based microgrids," *Automatica*, vol. 50, no. 10, pp. 2457–2469, 2014.

[13] A. H. Etemadi, E. J. Davison, and R. Iravani, "A decentralized robust control strategy for multi-DER microgrids part I: Fundamental concepts," *IEEE Transactions on Power Delivery*, vol. 27, no. 4, pp. 1843–1853, 2012.

[14] S. Riverso, F. Sarzo, and G. Ferrari-Trecate, "Plug-and-play voltage and frequency control of islanded microgrids with meshed topology," Dipartimento di Ingegneria Industriale e dell'Informazione, Università degli Studi di Pavia, Pavia, Italy, Tech. Rep., 2014. [Online]. Available: arXiv:1405.2421

[15] S. Riverso, M. Farina, and G. Ferrari-Trecate, "Plug-and-Play Decentralized Model Predictive Control for Linear Systems," *IEEE Transactions on Automatic Control*, vol. 58, no. 10, pp. 2608–2614, 2013.

[16] ——, "Plug-and-Play Model Predictive Control based on robust control invariant sets," *Automatica*, vol. 50, no. 8, pp. 2179–2186, 2014.

[17] S. Riverso, "Distributed and plug-and-play control for constrained systems," Ph.D. dissertation, Università degli Studi di Pavia, 2014. [Online]. Available: http://sisdin.unipv.it/pnpmpc/phpinclude/papers/phd_thesis_riverso.pdf

[18] J. Stoustrup, "Plug & play control: Control technology towards new challenges," *European Journal of Control*, vol. 15, no. 3, pp. 311–330, 2009.

[19] S. Bansal, M. Zeilinger, and C. Tomlin, "Plug-and-play model predictive control for electric vehicle charging and voltage control in smart grids," in *IEEE 53rd Conference on Decision and Control (CDC),*, 2014, pp. 5894–5900.

[20] X. Lu, J. M. Guerrero, K. Sun, and J. C. Vasquez, "An improved droop control method for DC microgrids based on low bandwidth communication with dc bus voltage restoration and enhanced current sharing accuracy," *IEEE Transactions on Power Electronics*, vol. 29, no. 4, pp. 1800–1812, 2014.

[21] J. Zhao and F. Dörfler, "Distributed control, load sharing, and dispatch in DC microgrids," in *American Control Conference (ACC)*, 2015, pp. 3304–3309.

[22] M. Andreasson, R. Wiget, D. Dimarogonas, K. Johansson, and G. Andersson, "Distributed primary frequency control through multi-terminal hvdc transmission systems," in *American Control Conference (ACC)*, 2015, pp. 5029–5034.

[23] D. Zonetti, R. Ortega, and A. Benchaib, "A globally asymptotically stable decentralized PI controller for multi-terminal high-voltage DC transmission systems," in *European Control Conference (ECC)*, 2014, pp. 1397–1403.

[24] V. Venkatasubramanian, H. Schattler, and J. Zaborszky, "Fast Time-Varying Phasor Analysis in the Balanced Three-Phase Large Electric Power System," *IEEE Transactions on Automatic Control*, vol. 40, no. 11, pp. 1975–1982, 1995.

[25] Q. Shafiee, T. Dragičević, J. C. Vasquez, and J. M. Guerrero, "Modeling, Stability Analysis and Active Stabilization of Multiple DC-Microgrid Clusters," in *Proceedings of the IEEE International Energy Conference (ENERGYCON)*, Dubrovnik, Croatia, May 13-16, 2014, pp. 1284–1290.

[26] K. J. Åström and T. Hägglund, *Advanced PID control*. ISA-The Instrumentation, Systems, and Automation Society; Research Triangle Park, NC 27709, 2006.

[27] M. Babazadeh and H. Karimi, "A Robust Two-Degree-of-Freedom Control Strategy for an Islanded Microgrid," *IEEE Transactions on Power Delivery*, vol. 28, no. 3, pp. 1339–1347, 2013.

[28] J. Lunze, *Feedback control of large scale systems*. Upper Saddle River, NJ, USA: Prentice Hall, Systems and Control Engineering, 1992.

[29] M. Tucci, S. Riverso, J. C. Vasquez, J. M. Guerrero, and G. Ferrari-Trecate, "A decentralized scalable approach to voltage control of DC islanded microgrids," Dipartimento di Ingegneria Industriale e dell'Informazione, Università degli Studi di Pavia, Pavia, Italy, Tech. Rep., 2015. [Online]. Available: arXiv:1503.06292

[30] H. Akagi, E. H. Watanabe, and M. Aredes, *Instantaneous power theory and applications to power conditioning*. Hoboken, New Jersey, USA: John Wiley & Sons, IEEE Press series on Power Engineering, 2007.

[31] P. Kokotovic, H. K. Khalil, and J. O'reilly, *Singular perturbation methods in control: analysis and design*. Siam, 1999, vol. 25.

[32] E. H. Abed, "Decomposition and stability for multiparameter singular perturbation problems," *Automatic Control, IEEE Transactions on*, vol. 31, no. 10, pp. 925–934, 1986.

[33] J. Schiffer, D. Goldin, J. Raisch, and T. Sezi, "Synchronization of droop-controlled microgrids with distributed rotational and electronic generation," in *Decision and Control (CDC), 2013 IEEE 52nd Annual Conference on*. IEEE, 2013, pp. 2334–2339.

[34] V. Mariani, F. Vasca, J. Vasquez, and J. Guerrero, "Model order reductions for stability analysis of islanded microgrids with droop control," *Industrial Electronics, IEEE Transactions on*, vol. 62, no. 7, pp. 4344–4354, July 2015.

[35] S. Skogestad and I. Postlethwaite, *Multivariable feedback control: analysis and design*. New York, NY, USA: John Wiley & Sons, 1996.

[36] S. Boyd, L. El Ghaoui, E. Feron, and V. Balakrishnan, *Linear matrix inequalities in system and control theory*. Philadelphia, Pennsylvania, USA: SIAM Studies in Applied Mathematics, vol. 15, 1994.

[37] G. H. Golub and C. F. Van Loan, *Matrix computations*. JHU Press, 2012, vol. 3.